Informes Técnicos Ciemat 1510
SETIEMBRE, 2022

LABORATORY TESTS ON BENTONITE HOMOGENISATION PERFORMED BY CIEMAT: GAP FILLING (PROJECT BEACON)

Villar Galicia, M. V.
Gutiérrez Álvarez, C.
Campos Martín, G.

GOBIERNO DE ESPAÑA
MINISTERIO DE CIENCIA E INNOVACIÓN
Ciemat
Centro de Investigaciones Energéticas, Medioambientales y Tecnológicas

Publication available in catalog of official publications

ISSN: 2695-8864
NIPO: 832-22-004-9

Edition and Publication:
Editorial CIEMAT
Avda. Complutense, 40 28040-MADRID
e-mail: editorial@ciemat.es
Editorial news

For an update of the interpretations included in this report, please check “Villar, M.V., Gutiérrez-Álvarez, C., Campos, G. 2022. Bentonite swelling into a void under suction and water flow. Acta Geotechnica”

ENSAYOS DE LABORATORIO SOBRE HOMOGENEIZACIÓN DE BENTONITA REALIZADOS EN CIEMAT: RELLENO DE HUECOS (PROYECTO BEACON)

Villar Galicia, M.V.; Gutiérrez Álvarez, C.; Campos Martín, G.

35 pp; 14 ref; 45 fig, 6 tbl; 1 an.

Resumen:

Se presenta un trabajo experimental desarrollado en el marco del almacenamiento geológico de residuos nucleares para mejorar la comprensión de los procesos de homogeneización de las barreras de bentonita en lo que se refiere al relleno de los huecos producidos durante su instalación. Bloques de bentonita FEBEX compactada se hidrataron bajo condiciones de hinchamiento axial limitado. Parte se saturaron por su parte superior (donde estaba el hueco) mediante la técnica de translación de ejes (imponiendo succión), y otras se hidrataron con agua por su base o a través del hueco superior. La hidratación fue más lenta en fase vapor, y la humedad de las muestras hidratadas bajo la succión mayor (6 MPa) fue menor, no siendo el hinchamiento desarrollado suficiente para rellenar el hueco. Sin embargo, el hinchamiento de las muestras saturadas bajo 0,5 MPa rellenó el hueco antes de que se alcanzase la humedad de equilibrio. Las muestras saturadas con agua líquida a partir del hueco se saturaron más rápidamente, por la posibilidad de hinchar libremente y desarrollar una zona de alta porosidad y permeabilidad. Al final de los ensayos, la humedad fue mayor y la densidad menor hacia la superficie de hidratación, pero estos gradientes resultaron más persistentes y acusados cuanto más rápida fue la hidratación.

LABORATORY TESTS ON BENTONITE HOMOGENISATION PERFORMED BY CIEMAT: GAP FILLING (PROJECT BEACON)

Villar Galicia, M.V.; Gutiérrez Álvarez, C.; Campos Martín, G.

35 pp; 14 ref; 45 fig, 6 tbl; 1 an.

Abstract:

To improve the understanding of the homogenisation process of bentonite barriers for geological disposal of nuclear waste, in particular with regards to the filling of technological voids, tests were performed with compacted FEBEX bentonite samples hydrated under limited axial swelling. The samples were saturated from the top surface using the vapour transfer technique (imposing suction), or with deionised water injected from the bottom surface or from the gap on top. Hydration was slower with water vapour than liquid water. The final water content of the samples tested under suction 6 MPa was lower and not enough to allow sufficient bentonite swelling to close the gap. In contrast, the samples saturated under suction 0.5 MPa reached higher water contents and were able to fill the gap before the equilibrium water content had been reached. In the tests performed with liquid water supplied through the gap, the samples saturated faster because they were able to swell into the open void and the higher-permeability swollen bentonite took water quickly. The final water content was higher and the dry density lower towards the hydration surface. These gradients were more remarkable and persistent as hydration was faster.

ACKNOWLEDGEMENTS

The research leading to these results was financed by the Beacon project, which receives funding from the Euratom Research and Training Programme 2014–2018 under grant agreement number 745942. Part of the laboratory work was carried out by J. Aroz. The mercury intrusion porosimetry tests were performed at the Petrophysical laboratory of CIEMAT by N. Brea.

CONTENTS

LIST OF FIGURES

LIST OF TABLES

1 INTRODUCTION

The only currently recognised practicable solution for final disposal of highly active and long-lived radioactive wastes is emplacement in a Geological Disposal Facility with a combination of natural and engineered barriers. Openings created during the construction of the repository are potential preferential pathways for water, gas and radionuclides migration and for this reason deposition galleries or holes and access galleries and shafts should be backfilled and sealed. Even so it seems inevitable that some voids and small openings –frequently referred to as technological or construction voids or gaps– are created during construction. The evidence provided by some large-scale in situ tests indicates that these voids will quickly seal if water availability is enough (García-Siñériz et al. 2015, Villar et al. 2020). However, under limited water supply, as may be the case in some argillaceous host rocks, the closing of gaps may take much longer. In both cases the bentonite mass redistribution necessary to fill the void may lead to barrier inhomogeneities in terms of water content and dry density of the bentonite. These might have repercussions on the subsequent performance of the barrier, since the thermo-hydro-mechanical properties of the bentonite depend mainly on its dry density and water content.

In this context, the overall objective of the BEACON (Bentonite Mechanical Evolution) project was to evaluate the consequences of heterogeneities on the performance of bentonite barriers in geological repositories for high-level radioactive waste. As a contribution to this project, CIEMAT performed a series of tests to follow the density and water content changes in compacted bentonite samples saturated under limited axial swelling conditions and at the same time observe the closing of the initial gap. Two factors potentially affecting the closing of voids were analysed: water availability and gap location. Thus, the tests were performed either under constant water pressure conditions, simulating a repository excavated in crystalline host rock with plenty of water, or under controlled suction, simulating a repository with scarce water availability. FEBEX bentonite initially compacted with its hygroscopic water content (~14%) at a nominal dry density of 1.7 g/cm^3 was used in all the tests. The hydration of the samples took place with water in the vapour phase through the sample surface closest to the gap (GAP-vapour tests), and with liquid water (GAP-liquid), either through the sample surface away from the gap or from the gap surface.

The set of tests presented in this paper has been used in a modelling benchmark of the SKB project Task Force on Engineered Barriers. They have also been published in Villar et al. (2022).

2 MATERIAL

FEBEX bentonite has been used in all the tests. It is a 900-t batch of bentonite extracted from the Cortijo de Archidona quarry (Almería, Spain) and processed in 1996 for the FEBEX project. The processing consisted in homogenisation, air-drying and manual removing of volcanic pebbles on-site and, at the factory, crumbling, drying in a rotary oven at clay temperatures between 50 and 60 °C and sieving through a 5-mm mesh. The physico-chemical properties of the FEBEX bentonite, as well as its most relevant thermo-hydro-mechanical and geochemical characteristics obtained during the FEBEX project were summarised in e.g. ENRESA (2006) and updated in e.g. Villar (2017).

The smectite content of the FEBEX bentonite is close to 90 wt.%. The smectitic phases are actually made up of a montmorillonite-illite mixed layer, with 10-15 wt.% of illite layers. Besides, the bentonite contains variable quantities of quartz (2±1 wt.%), plagioclase (3±1 wt.%), K-felspar (traces), calcite (1 wt.%) and cristobalite–trydimite (2±1 wt.%). The cation exchange capacity is 98±2 meq/100 g, the main exchangeable cations being calcium (33±2 meq/100 g), magnesium (33±3 meq/100 g) and sodium (28±1 meq/100 g). The predominant soluble ions are chloride, sulphate, bicarbonate and sodium.

The liquid limit of the bentonite is 102±4 %, the plastic limit 53±3 %, the density of the solid particles 2.70±0.04 g/cm^3, and 67±3 % of particles are smaller than 2 µm. The hygroscopic water content in equilibrium with the laboratory atmosphere (relative humidity 50±10 %, temperature 21±3 °C) is 13.7±1.3 %. The external specific surface area is 67 m^2/g and the total specific surface area is about 725±47 m^2/g.

The swelling pressure (P_s, MPa) of FEBEX samples flooded with deionised water up to saturation at room temperature and constant volume conditions can be related to dry density (ρ_d, g/cm^3) through the following equation (Villar, 2002):

$$\ln P_s = 6.77\rho_d - 9.07 \quad [1]$$

The difference between experimental values and this fitting is, on average, 25 percent.

The hydraulic conductivity (k_w) of the bentonite at room temperature is also exponentially related to its dry density, according to the following empirical expressions:

for dry densities of less than 1.47 g/cm^3:

$$\log k_w = -6.00\ \rho_d - 4.09 \quad [2]$$

for dry densities in excess of 1.47 g/cm^3:

$$\log k_w = -2.96\ \rho_d - 8.57 \quad [3]$$

The variation in the experimental values with respect to these fittings is smaller for low densities than it is for higher values, with an average –in absolute values– of 30 percent.

Relationships between suction and water content obtained for different bentonite dry densities under isochoric conditions can be found in Villar (2007), Villar et al. (2012, 2019). For a sample compacted at dry density 1.6 g/cm^3 with hygroscopic water content the initial suction value would be ~120 MPa.

3 METHODOLOGY

The objective of these tests was to follow the density, water content and microstructural changes in a block sample saturated under limited axial swelling conditions and at the same time observe the closing of the initial gap. FEBEX bentonite samples were compacted inside stainless steel rings and a gap was left on top. In all cases the granulated bentonite was initially compacted with its hygroscopic water content (~14 %) at a target dry density of 1.7 g/cm^3. These samples were hydrated with water either in vapour (GAP-vapour) or liquid phase (GAP-liquid) and were dismantled after different periods of time. The final water content and dry density of the bentonite at different levels of the sample were measured, as well as the pore size distribution.

3.1 GAP-VAPOUR TESTS

In the GAP-vapour tests the samples were compacted in a cell with perforated lids, and saturated from the top surface, where the gap was, using the vapour transfer technique (Figure 1), which consists in subjecting the sample to a certain relative humidity in a close container (vacuum desiccator). The diameter of the samples was 3.8 cm and the initial height was 2.5 cm. The bottom part of the cell was sealed, and on the top surface of the sample a porous ceramic filter was placed, so that water transfer took place through this porous medium. The initial gap thickness was of 0.5 cm. The evolution over time of the gap closing and the changes in bentonite overall water content and dry density were followed by periodically measuring the gap height and weighing the cylinder with the sample inside (Figure 2). A total of 26 cells were tested and dismantled at different periods of time between 15 days and 15.5 months. The samples were subjected to relative humidities corresponding to total suctions of 6 and 0.5 MPa keeping a constant temperature of 20 °C. These suctions were obtained by placing in the desiccators a sulphuric acid solution of concentration 10% and a sodium chloride solution of concentration 0.6 %, respectively.

The tests were performed at a temperature of 20.0±1.0 °C.

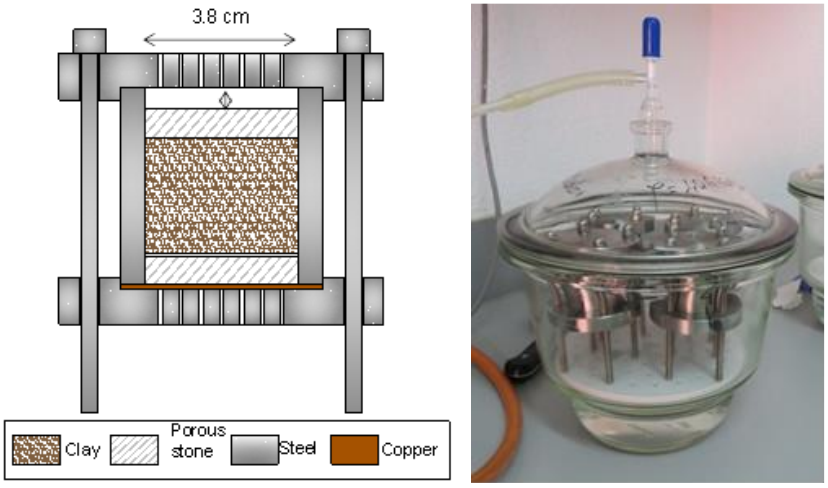

Figure 1. Schematic representation of the GAP-vapour test cells and desiccator with cells inside

Figure 2. Intermediate measurement of gap height in GAP-vapour tests

3.2 GAP-LIQUID TESTS

In the GAP-liquid tests the bentonite was saturated with water in the liquid phase under a very low flow rate either from the bottom surface, opposite to the gap or from the gap surface (as in the GAP-vapour tests). The initial characteristics of the samples were the same in both cases for all the tests: the bentonite was compacted with its hygroscopic water content (14.0±0.5 %) inside the cell ring applying a uniaxial pressure of ~30 MPa, giving place to an initial dry density of 1.67±0.02 g/cm^3. The diameter of the resulting samples was 50 mm and the initial height 2.54±0.02 cm, leaving a gap of 0.88±0.02 cm on top of them. Note that the difference in gap height with respect to the GAP-vapour tests (0.9 vs 0.5 cm) allowed larger maximum swelling. The sample was sandwiched between porous ceramic filters (Figure 3).

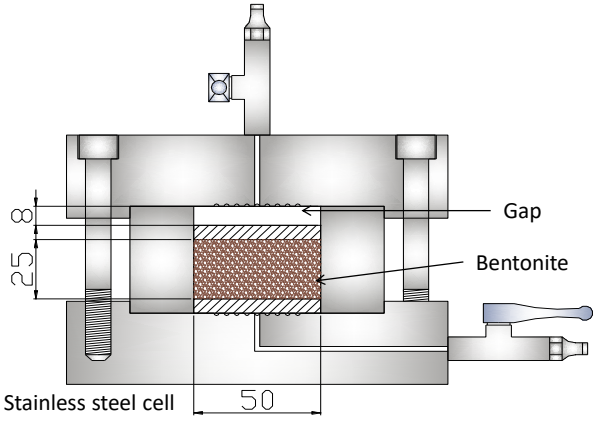

Figure 3. Blueprint of the cell for the GAP-liquid tests with the sample inside

Deionised water was injected either through the bottom or through the top with a pressure/volume controller at a rate of 0.072 cm^3/h, the minimum allowed by the equipment, so that to avoid interference with the sample swelling and to make the process as slow as possible. The part of the cell opposite to the hydration surface was open to atmosphere (Figure 4 shows the configuration for the tests with water injection opposite to the gap). In the set of tests with saturation through the gap (except in the first one, GL6), the porous stone was saturated outside

the cell prior to the start of the test. Injection pressure was atmospheric at the beginning of the tests. Both injection pressure and water intake were measured online.

The tests were performed at laboratory temperature (22.9±1.6 °C). The results of 13 dismantled tests are presented in this document.

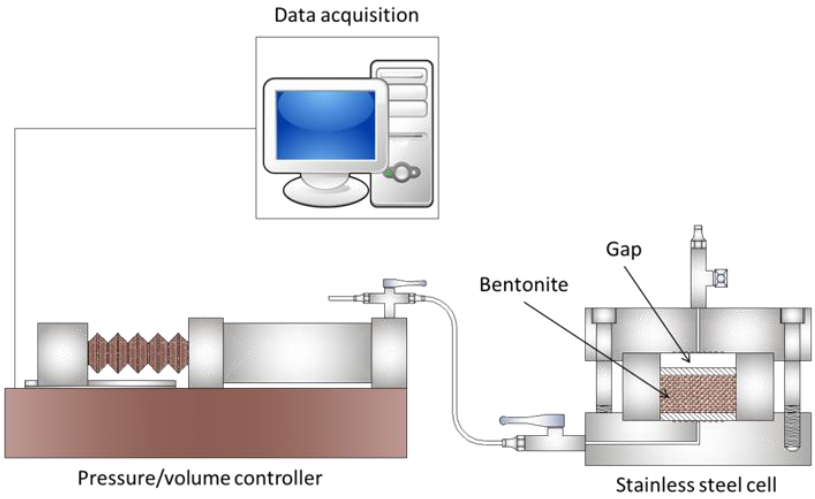

Figure 4. Schematic representation of the assembly for GAP-liquid tests (injection opposite to gap)

3.3 POSTMORTEM TESTS

At the end of the two kinds of tests the samples were measured, weighed, and cut into transversal sections (Figure 5). Three sections were usually defined, because a minimum section volume was necessary to obtain subsamples coherent enough to determine their dry density. In each section subsamples were obtained to determine water content, dry density and pore size distribution (Figure 6, left). In the GAP-liquid tests with saturation through the gap, it was observed that the periphery of the samples seemed drier than the internal part. For this reason, the transversal sections were subsampled in a different way, considering the internal and external parts (Figure 6 , right).

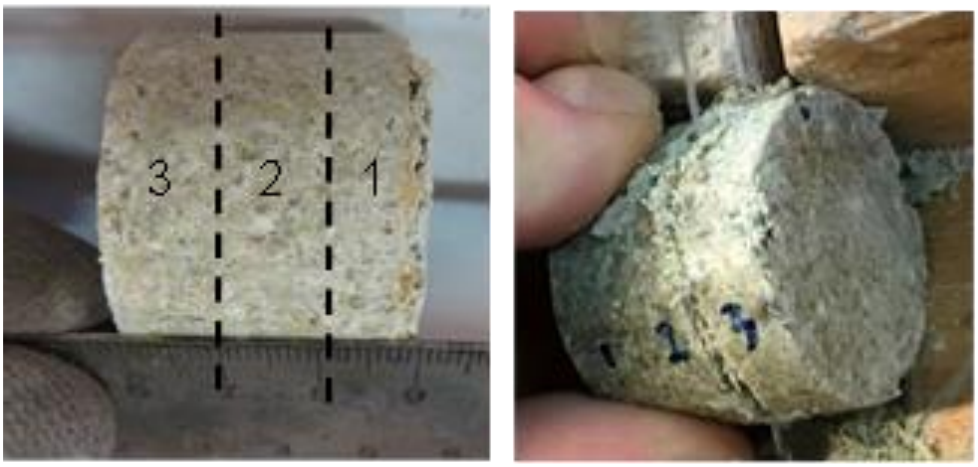

Figure 5. Final subsampling after extraction of samples from the GAP tests cells

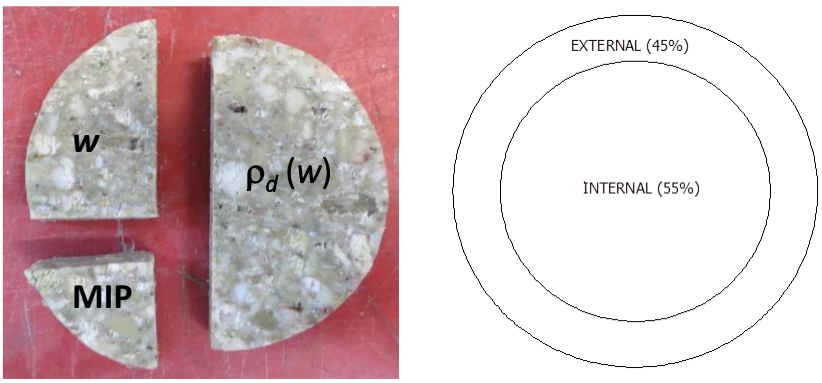

Figure 6. General subsampling of sections for postmortem determinations (left) and subsamples of a section for postmortem determinations in the GAP-liquid tests with injection through the gap (right)

Dry density (ρ_d) is defined as the ratio between the mass of the dry sample and the volume occupied by it prior to drying. The volume of the specimens after extraction from the cell was determined by measuring their dimensions, whereas the volume of the subsamples of each section was determined by immersing them in a recipient containing mercury and by weighing the mercury displaced, considering a density of mercury of 13.6 g/cm^3. The precision of this measurement is between 0.01 and 0.02 g/cm^3. The mass of water was determined as the difference between the mass of the sample and its mass after oven drying at 110 °C for 48 hours. The gravimetric water content (w) is defined as the ratio between the mass of water and the mass of dry solid expressed as a percentage. The precision of this measurement is about 0.2 %. The water content was usually determined in the subsamples used for the dry density determination and also in an additional subsample of each section (Figure 6).

The pore size distribution of the subsamples was determined by mercury intrusion porosimetry (MIP). The mass of the subsamples used was between 2.54 and 0.54 g. The samples were put in the ice condenser of a Telstar LioQuest equipment at -30 °C for 3 hours. Subsequently, they were lyophilised for 22 hours at a temperature of -50 °C under a vacuum of 0.2 mbar, so that to eliminate the water in the pores by sublimation. Thereafter, they were heated at 25-30 °C for 3 hours. The samples were later kept in a desiccator until the MIP analysis. The porosimeter used was a Micromeritics AutoPore Series IV 9500, which allowed the exploration of pore diameters between 0.007 and 550 µm. Prior to mercury injection the sample was outgassed by applying a vacuum of 50 µm-Hg. Afterwards the mercury injection pressure was increased from 2.7 kPa to 220 MPa in 109 steps. To determine the extrusion branch of the curve, the pressure was released in 56 steps down to a pressure of 68.6 kPa. A contact angle of mercury of 139° both on advancing and of receding on the clay surface was considered.

4 RESULTS

4.1 GAP-VAPOUR TESTS

4.1.1 EVOLUTION OVER TIME

The GAP-vapour cells were checked every week. For that, the lids were unscrewed and the cell with the sample inside was weighed and the height of the gap measured (Figure 2). In this way, the evolution over time of the overall bentonite water content and dry density was approximately followed, as reported in the Tables included in the Annex (Table A- 1 to Table A- 5 and Table A- 8 to Table A- 13). Since the bentonite was compacted with hygroscopic water content, the initial suction of the samples was very high, about 100 MPa. For this reason all the samples took water under the two suctions applied (6 and 0.5 MPa), swelled and tended to close the gap. Figure 7 and Figure 8 show the evolution of the overall water content and dry density of the samples in the tests performed under suctions 6 and 0.5 MPa. All the tests were performed in duplicate, and in most cases the results of the two samples were coherent.

The initial and final values of dry density and water content for each test performed under the two different suctions are shown in Table 1 and Table 2 and the final values are plotted in Figure 9. In the first stages, for times shorter than 40 days, the samples under 6 MPa took more water and swelled more. For longer equilibration times the trend inverted and consequently the final water contents of samples under 0.5 MPa were higher and their dry densities lower. After approximately 300 days the equilibrium water content for a suction of 6 MPa was reached (~27%). The gap was not completely closed in the tests performed under 6 MPa, which indicates that the swelling capacity of the bentonite under this suction was lower than 20%. In the tests performed under 0.5 MPa, the gap was closed at a time between 100 and 180 days (from that time on the dry density reached its lower possible value). Also, for suction 0.5 MPa the water content remained constant after less than 200 days (~34%), which is probably related to the fact that no further swelling was allowed.

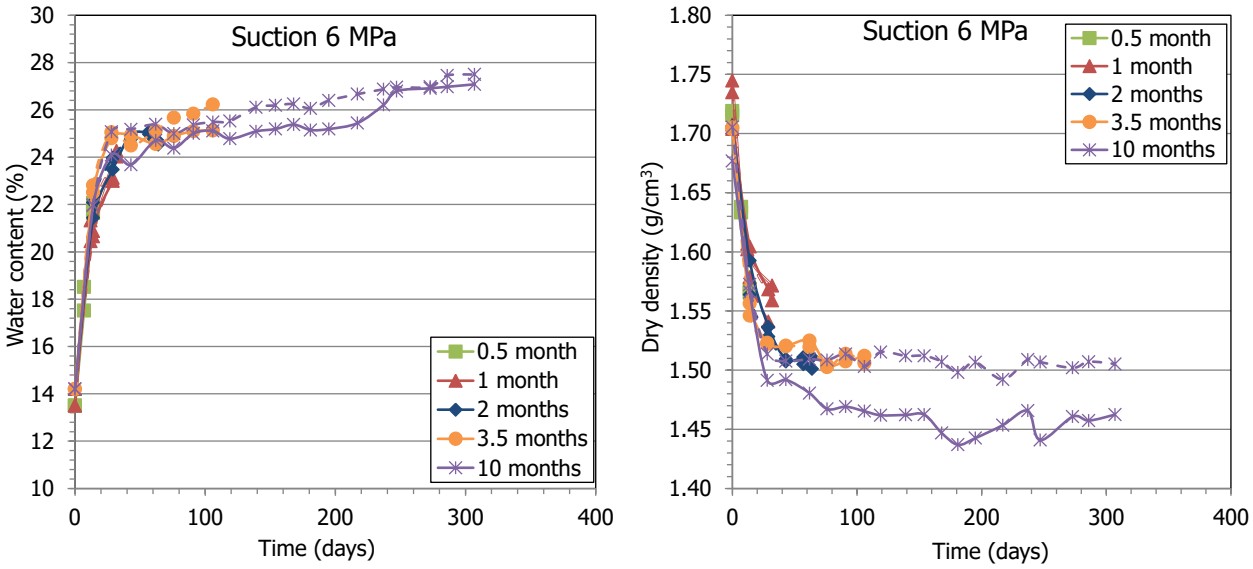

Figure 7. Evolution of water content and dry density in GAP-vapour tests under suction 6 MPa

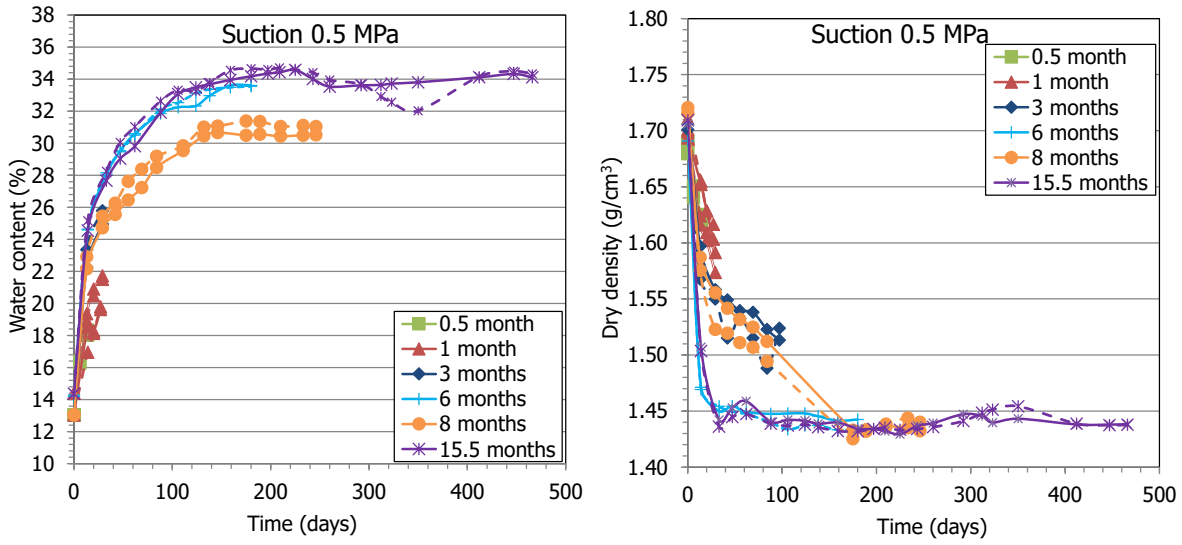

Figure 8. Evolution of water content and dry density in GAP-vapour tests under suction 0.5 MPa

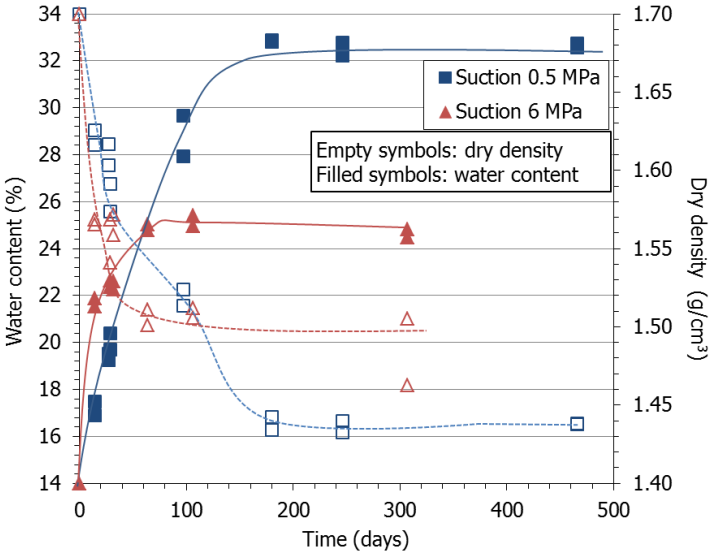

Figure 9. Final results of dry density and water content in GAP-vapour tests

Sample	Time (days)	Initial *w* (%)	Initial ρ_d (g/cm^3)	Initial gap (mm)	Final *w* (%)	Final ρ_d (g/cm^3)	Final gap (mm)	Final *Δ h/ho* (%)
9	14	13.5	1.72	4.77	21.5	1.57	2.21	9.6
10	14	13.5	1.72	5.06	21.9	1.57	2.50	9.6
3	29	14.2	1.71	4.59	22.4	1.57	2.20	8.9
4	29	14.2	1.70	4.85	22.6	1.54	2.02	10.6
11	32	13.5	1.74	5.20	22.6	1.57	2.34	11.0
12	32	13.5	1.73	5.31	22.3	1.56	2.37	11.3
1	64	14.2	1.70	4.89	24.8	1.51	1.52	12.8
2	64	14.2	1.71	4.89	25.0	1.50	1.30	13.7
6	106	14.2	1.71	4.68	25.0	1.51	1.31	12.8
7	106	14.2	1.70	5.08	25.4	1.51	1.62	13.2
5	307	14.2	1.68	4.90	24.5	1.46	1.02	14.7
8	307	14.2	1.71	5.08	24.8	1.51	1.61	13.3

Table 1. Initial and final overall water content (w) and dry density (ρ_d) of the GAP-vapour samples tested under 6 MPa

Sample	Time (days)	Initial *w* (%)	Initial ρ_d (g/cm^3)	Initial gap (mm)	Final *w* (%)	Final ρ_d (g/cm^3)	Final gap (mm)	Final *Δ h/ho* (%)
19	14	13.1	1.69	4.39	17.5	1.63	3.23	4.0
20	14	13.1	1.68	4.51	16.9	1.62	3.37	3.9
17	27	13.1	1.69	4.37	19.5	1.60	2.80	5.6
18	27	13.1	1.71	5.04	19.3	1.62	3.42	5.8
21	29	14.4	1.70	4.60	20.4	1.57	2.40	8.1
22	29	14.4	1.70	4.77	19.7	1.59	2.92	6.8
15	97	13.1	1.71	4.91	27.9	1.51	1.44	13.3
16	97	13.1	1.70	5.07	29.7	1.52	1.99	11.6
23	180	14.4	1.69	4.45	32.9	1.44	0.00	17.2
24	180	14.4	1.71	4.82	32.8	1.43	0.00	19.0
13	246	13.1	1.72	5.14	32.2	1.43	0.07	19.8
14	246	13.1	1.72	5.08	32.8	1.44	0.10	19.5
25	466	14.4	1.71	4.82	32.6	1.44	0.02	18.6
26	466	14.4	1.71	4.92	32.7	1.44	0.05	18.9

Table 2. Initial and final overall water content (w) and dry density (ρ_d) of the GAP-vapour samples tested under 0.5 MPa

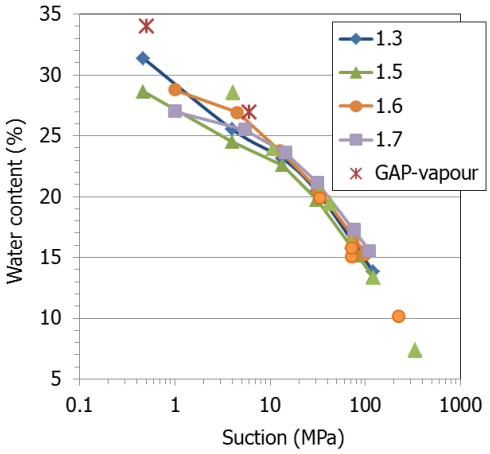

Figure 10. Equilibrium values reached in the GAP-vapour tests and water retention curves of FEBEX bentonite compacted to different dry densities (indicated in g/cm^3) obtained under isochoric conditions (results from Villar 2007, Villar et al. 2012 and unpublished)

4.1.2 FINAL PHYSICAL STATE

After different equilibration times the cells were dismantled, the bentonite weighed and measured and cut into sections for the postmortem determinations, as described in chapter 3.3.

Figure 11 shows the appearance of some of the samples at the end of the tests, with the top of the sample presenting a crumbled, uneven surface because of the free swelling. The results obtained for the different subsamples in terms of water content and dry density are detailed in the Annex (Table A- 6 and Table A- 14) and plotted in Figure 12 and Figure 13. The shorter tests showed a water content gradient from top to bottom. Towards the top of the sample, where the gap was, the water content was higher and the dry density lower. In fact, the upper surface of the sample crumbled easily, since it swelled into a void (see Figure 11). For this reason it was difficult in some

cases to cut the upper subsamples and determine their dry density, which was lower. The dry density gradients kept even in the longer tests, although in the samples tested under suction 0.5 MPa were less steep and kept more or less constant as the overall water content increased and the overall dry density decreased. This could be explained by the slowness of the saturation process under the lowest suction (Figure 9).

Figure 11. Appearance of samples after extraction of the cells and subsampling for postmortem analyses

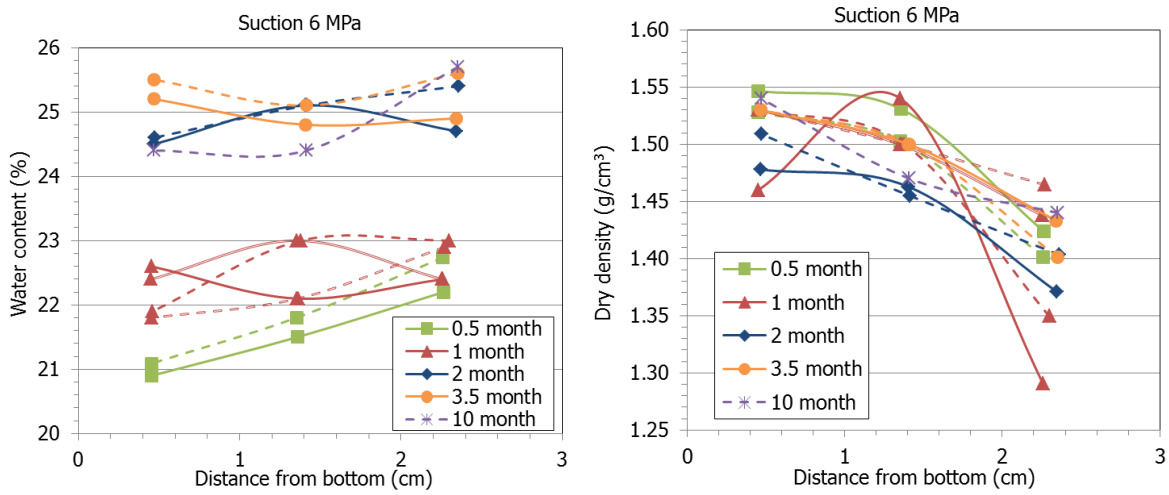

Figure 12. Final water content and dry density of subsamples of the tests performed under suction 6 MPa

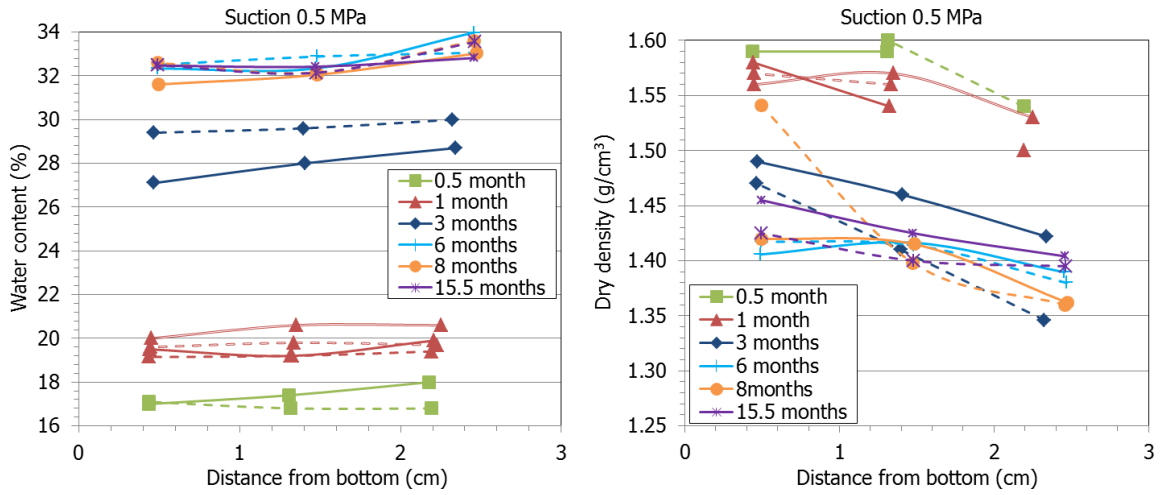

Figure 13. Final water content and dry density of subsamples of the tests performed under suction 0.5 MPa

4.1.3 PORE SIZE DISTRIBUTION

From each cell three other subsamples taken at different distances from the gap were used to determine the pore size distribution by MIP (Figure 5, left). Figure 14 and Figure 15 show the incremental curves of mercury intrusion as a function of the mean pore diameter of the diameter size intervals corresponding to each pressure increase step of the samples from these cells. The curve corresponding to a FEBEX sample compacted with approximately the same dry density and water content as the initial conditions used in the cells (1.69 g/cm^3, 13.5%) is also included (labelled "Initial"). The determination was performed in the subsamples of all the cells (Table A- 7, Table A- 15), but only those corresponding to the shorter and longer tests performed under each suction are shown in these Figures (the other Figures are included in the Annex, Figure A- 1, Figure A- 2). For all the samples there were two pore families corresponding approximately to pores larger and smaller than 200 nm with diameter modes of 19 µm and 11 nm, respectively. In several THM models, this pore size represents the limit separating inter-aggregate from intra-aggregate pores, the latter not affected by density changes (e.g. Sánchez et al. 2005). There is discussion on the criteria that can be followed to select this delimiting value (Yuan et al. 2020). The 'valley' criterion was chosen in this work, consisting of using the lowest point of the valley between the two peaks of a bimodal distribution. According to the usual pore size classification (Sing et al. 1985), the first family identified would be in the range size of the macropores (larger than 50 nm) and the second one in that of the mesopores (between 50 and 2 nm). The Figures show that the volume of pores larger than 200 nm increased during testing, particularly as the test was longer. The mean size of the macropores also tended to increase, from an initial diameter mode of 19 µm to values of up to 80 µm in the tests under suction 0.5 MPa and up to 100 µm in the tests under suction 6 MPa, in both cases with a few subsamples of the shorter tests showing much higher sizes (Figure 16 and Figure A- 3). The mode of the mesopores did not change much with respect to the original value, remaining in sizes of 12±4 nm with no particular trends.

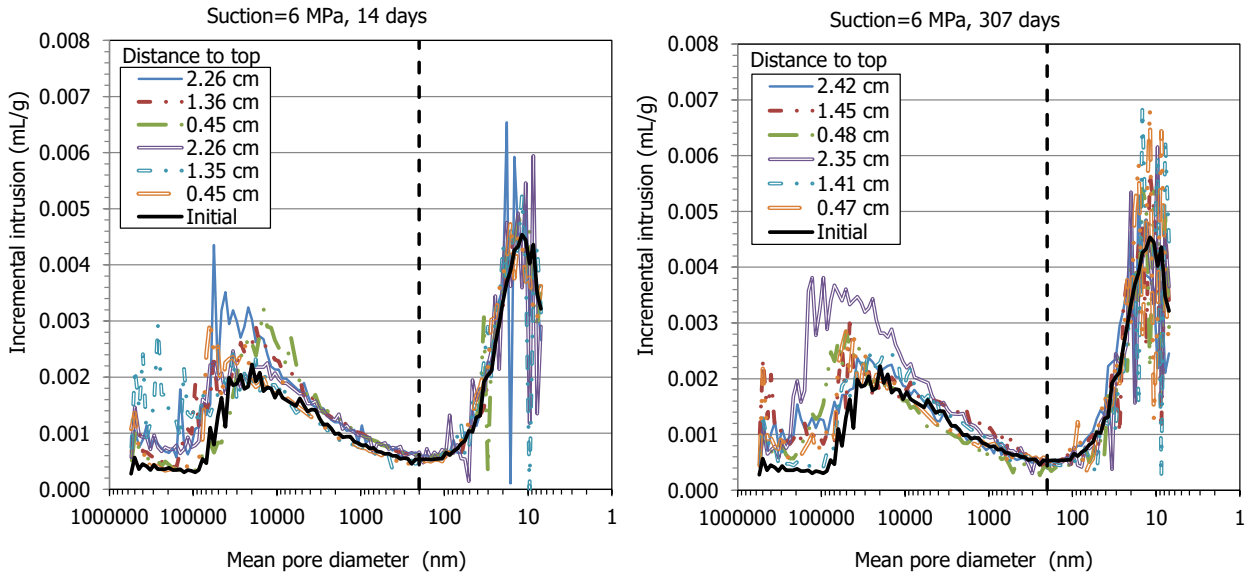

Figure 14. Pore size distribution of subsamples tested in GAP-vapour cells under suction 6 MPa for two different times and for the initial block expressed as incremental mercury intrusion (duplicate samples for each duration)

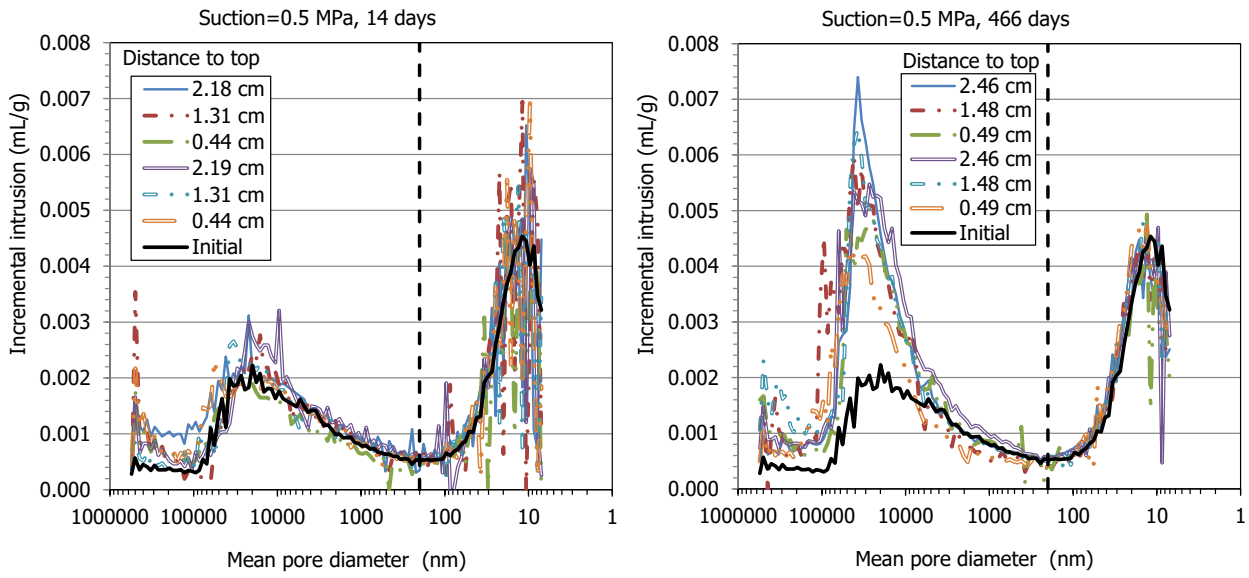

Figure 15. Pore size distribution of subsamples tested in GAP-vapour cells under suction 0.5 MPa for two different times and for the initial block expressed as incremental mercury intrusion (duplicate samples for each duration)

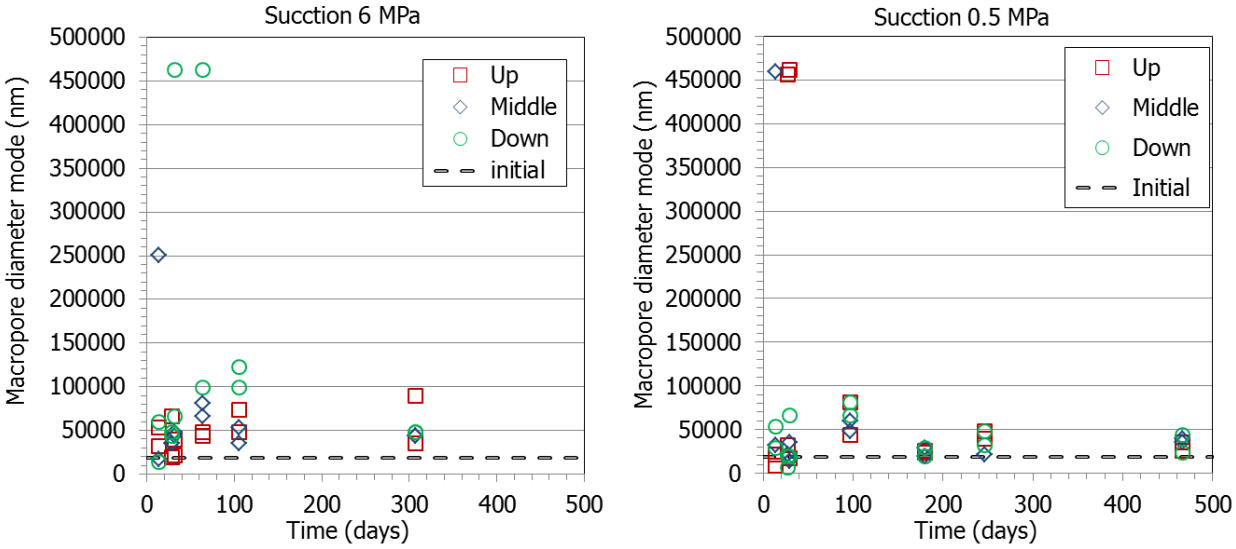

Figure 16. Mode size of macropores of subsamples tested in GAP-vapour cells under suction 6 MPa (left) and 0.5 MPa (right) for different times and as a function of the position of the subsample (up: closest to the gap; duplicate samples for each duration). The dotted horizontal line indicates the value for the initial sample

The mercury intrusion method allows access to be gained only to part of the macroporosity (pores of diameter smaller than ~550 µm) and to part of the mesopores (those of diameters larger than 7 nm), since mercury does not intrude the microporosity (pores of a size of less than 2 nm, according to Sing et al. (1985)). An estimation of the percentage of pores actually intruded can be made by comparing the actual void ratio of the samples (computed from their dry density and density of solid particles) and the apparent void ratio calculated from mercury intrusion by the equipment software. Thus, the percentage of pores intruded by mercury in these subsamples was between 42 and 74%. The non-intruded porosity is usually associated in compacted clays to the pores of a size smaller than the limit of the apparatus (7 nm). There is uncertainty in this approach,

since it is possible that pores larger than 7 nm were not intruded because of the bottleneck effect. All of the volume of such pores will be allocated to the threshold radius class of the most restricted part of the entryway, which will result in an overestimation of the smaller pore sizes volume. Likewise, although in compacted clay materials pores larger than those that can be quantified by MIP are not expected, pores of this size could be present in the samples closest to the gap of the shorter tests, which were friable and crumbly. A visual inspection of the samples upon dismantling allowed to conclude that this was the case for the upper part of the samples shown in Figure 17, all of them corresponding to tests shorter than 32 days.

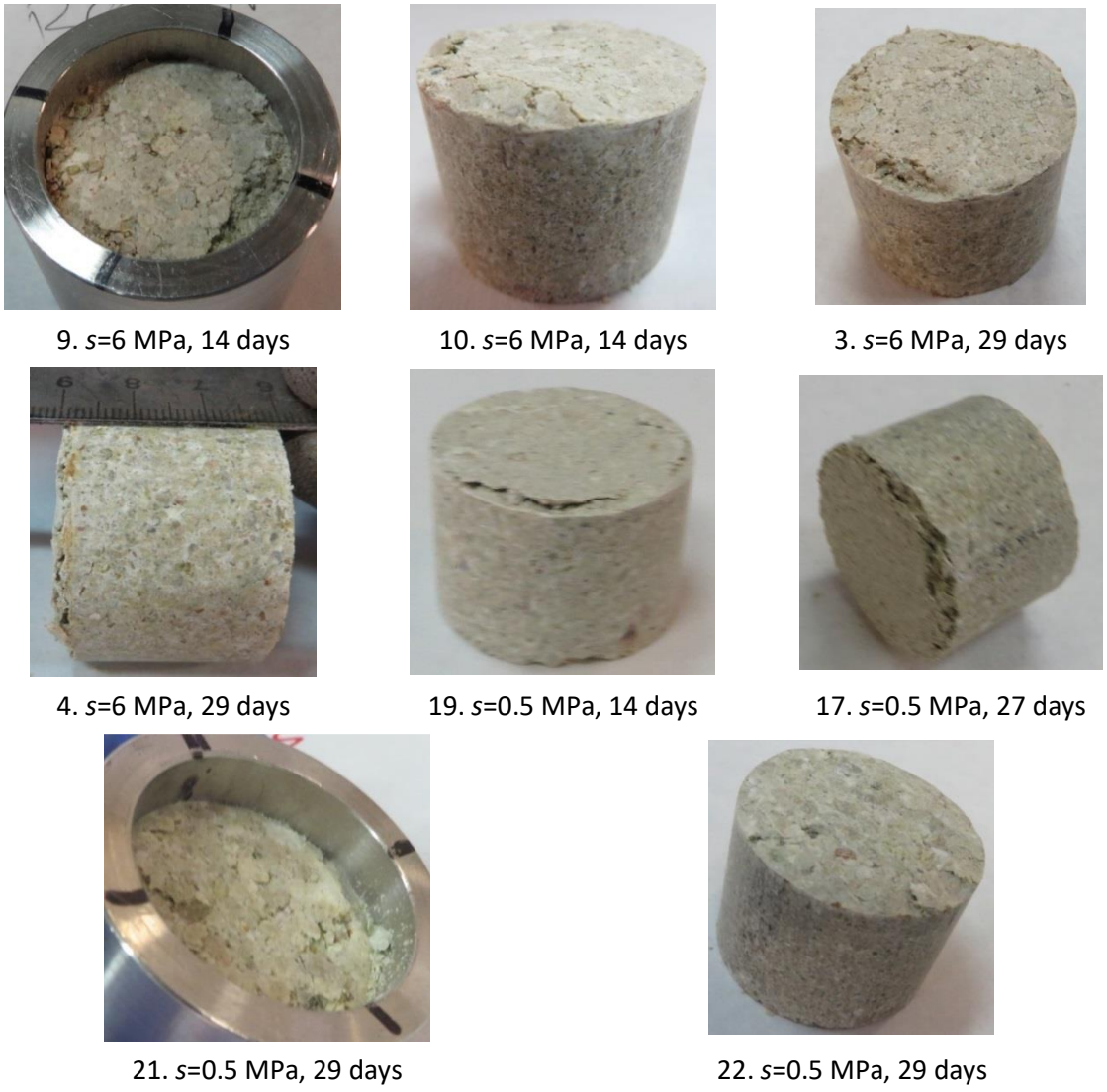

9. *s*=6 MPa, 14 days | 10. *s*=6 MPa, 14 days | 3. *s*=6 MPa, 29 days

4. *s*=6 MPa, 29 days | 19. *s*=0.5 MPa, 14 days | 17. *s*=0.5 MPa, 27 days

21. *s*=0.5 MPa, 29 days | 22. *s*=0.5 MPa, 29 days

Figure 17. Appearance upon dismantling of some of the shorter GAP-vapour tests

Hence, to take into account the large pores observed in those upper subsamples, an estimation of the volume of pores larger than 550 µm has been made following this approach (Villar et al. 2021).

At the beginning of a MIP test the calibrated sample holder is filled with mercury under a low injection pressure. Considering the sample mass and the volumes of the sample holder and of mercury intruded, the dry density of the sample is computed by the equipment software. This initial mercury injection is considered by the equipment as the zero value for the rest of the MIP test, which actually starts when injection pressure is increased above this value. Thus, all the large

porosity filled during this initial step is disregarded. The comparison between the dry density determined by the equipment at this step and the actual dry density of the sample allows computing the volume of pores larger than 550 μm: when the sample contains a significant volume of large pores, the dry density determined by the porosimeter is considerably higher than the actual dry density of the sample, whereas if there are not large pores the two values tend to be similar.

Taking all the above into account, the void ratio corresponding to pores larger and smaller than 200 nm (e_M and e_m, macro and micro, respectively) was recalculated, assuming that the non-intruded porosity corresponded to pores smaller than the equipment injection capacity and, in some upper subsamples, also to pores larger than 550 μm. The values are plotted in Figure 18 and Figure 19 for subsamples of the specimens tested under suctions 6 and 0.5 MPa, respectively. In all cases the largest proportion of void ratio corresponded to the pores of diameter smaller than 200 nm, the volume of which increased during testing with respect to the reference sample. Also, the percentage of void ratio corresponding to pores larger than 200 nm increased with respect to the reference sample, since the total void ratio increased because of the bentonite swelling into the gap and overall dry density decrease. In fact, the highest increase in void ratio was experienced by the samples closest to the gap, which agrees with their lower dry density (Figure 12 and Figure 13). The overall void ratio increase took place very quickly in the samples tested under 6 MPa (it was already clear after 15 days) but took longer in the samples tested under suction 0.5 MPa. This agrees with the different hydration kinetics of the two sets of tests commented above and would indicate that hydration under free swelling conditions brought about an increase in the volume of all pore sizes. Furthermore, in all the tests performed under suction 6 MPa the macropore void ratio was higher in the subsample closest to the gap than in the other subsamples. In contrast, this difference among subsamples was less clear in the longer tests performed under suction 0.5 MPa.

The ratio between the void ratio corresponding to pores smaller (e_m) and larger (e_M) than 200 nm is plotted on the right hand side of the Figures. This ratio was lower in the subsample closest to the gap for the tests shorter than 2 months performed under suction 6 MPa, whereas it remained similar to the initial one in the rest of subsamples. In the shorter tests ($\leq$3 months) performed under suction 0.5 MPa, this ratio increased at the bottom and tended to decrease towards the part of the samples closest to the hydration surface (gap), which would mean that the percentage of macropores increased in the most hydrated bentonite. Over time these differences inside a given sample were obliterated by the increase in void ratio corresponding to larger pores. As a result, all the subsamples from larger tests ($\geq$6 months), those in which the gap was closed, had e_m/e_M ratios lower than the initial one and similar among them, which would be an additional indication of equilibrium being reached.

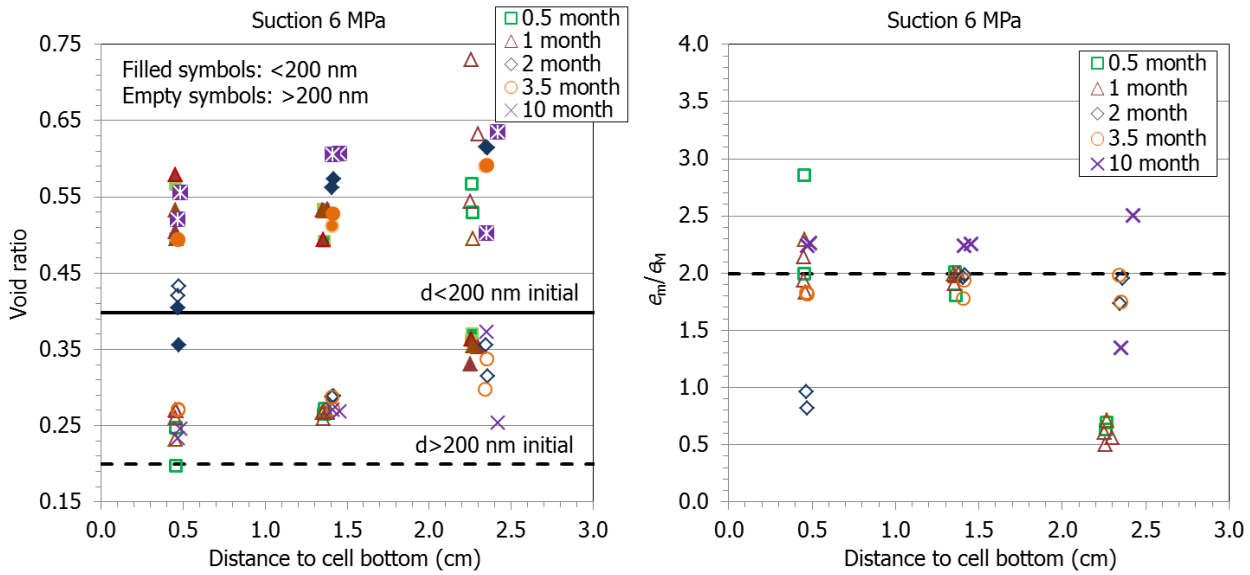

Figure 18. Void ratio corresponding to pores smaller (e_m) and larger than 200 nm (e_M) obtained by MIP in samples tested under suction 6 MPa (left) and ratio between both (right). The thick horizontal lines indicate the values for the initial sample (time=0)

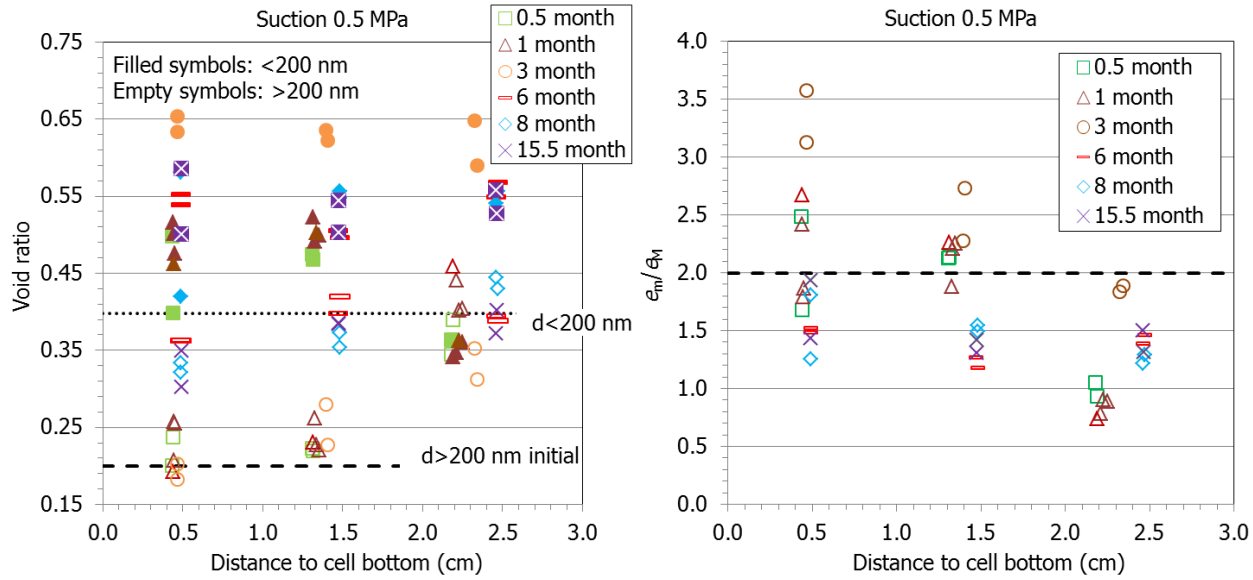

Figure 19. Void ratio corresponding to pores smaller (e_m) and larger than 200 nm (e_M) obtained by MIP in samples tested under suction 0.5 MPa (left) and ratio between both (right). The thick horizontal lines indicate the values for the initial sample (time=0)

The evolution of void ratio over time corresponding to pores larger and smaller than 200 nm can be seen in Figure 20 as a function of the position along the sample for the two suction values. In the tests under suction 0.5 MPa, close to the gap the macropore void ratio quickly increased, but then remained almost constant. In the middle part of the sample the increase in macropore void ratio was more gradual and reached a maximum after 180 days (when the gap was already closed), remaining constant afterwards. For the bottom part of the sample the increase in macropore void ratio took place only after 100 days. The increase in micropore void ratio was more uniform across a given sample, had a maximum after 97 days (once the gap was closed) and then remained approximately constant. In the tests under suction 6 MPa, there was a quick and huge increase in macropore void ratio close to the gap that was reduced after two months and

then did not change much. Figure 21 shows the appearance of the upper part of two of the samples saturated under suction 6 MPa after 14 days and just before dismantling after more than 100 days. It is clear that the initial disruption of the sample, likely with creation of macropores, was healed over time. The middle and bottom parts of the samples behaved similarly over time, with the pores <200 nm accounting for most of the overall increase in void ratio.

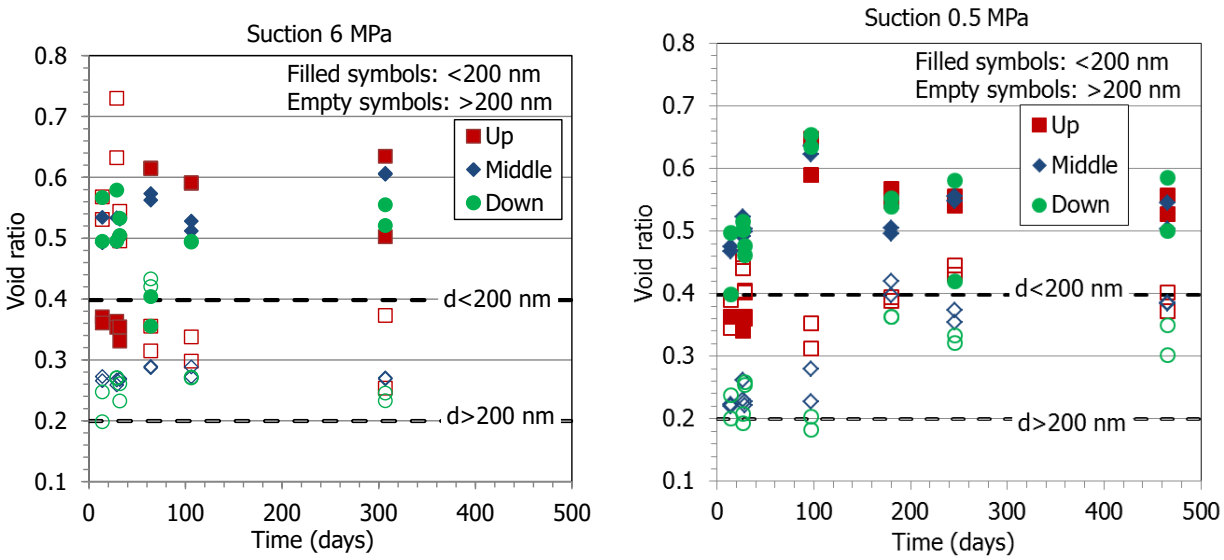

Figure 20. Evolution of void ratio over time corresponding to pores larger and smaller than 200 nm for the two sets of GAP-vapour tests. The dotted horizontal lines indicate the values for the initial sample (time=0)

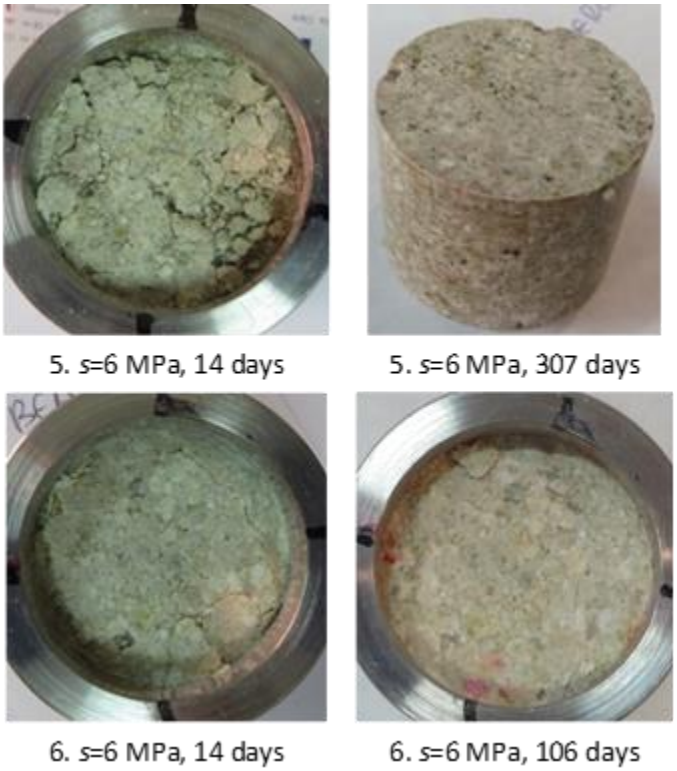

Figure 21. Appearance of two GAP-vapour samples saturated under suction 6 MPa at an intermediate stage (14 days, left column) and just before dismantling them (right column)

4.2 GAP-LIQUID TESTS

The tests in which the bentonite was saturated with liquid water were performed either injecting the water from the surface of the block opposite to the gap, or from the gap surface. The results of these two sets of tests are described separately. The initial characteristics of the samples were the same in both cases for all the tests: hygroscopic water content, nominal dry density of 1.7 g/cm^3, nominal height of 2.5 cm, a gap of 8 mm on top of them (Figure 3). For the GAP-liquid tests only the state of the sample at the end of each test is available, because their state could not be periodically checked without disturbing too much the state of the samples.

4.2.1 INJECTION OPPOSITE TO THE GAP

Six tests of the same initial characteristics were performed and dismantled after different hydration times (Table 3). In contrast to the GAP-vapour tests, the gap in these GAP-liquid tests was in the opposite side to the hydration surface. It was observed that the injection pressure (Figure 22), which was null at the beginning of the experiments, started to increase after ~7 days from the beginning of water injection, which was necessary to keep the flow rate imposed (0.07 cm^3/h). The overall degree of saturation of the samples when the injection pressure started to increase was between 57 and 74%. In all cases the upper outlet remained open to atmosphere during the whole duration of the test, except in the case of the longest one (GL1). In this test the injection pressure increased up to 2 MPa before a blackout made the injection pressure decrease. When the system was re-started the upper outlet was closed because water was flowing out. The tables with the numerical values of the pressure and water intake during the tests are included in the Annex (Table A- 16 to Table A-21).

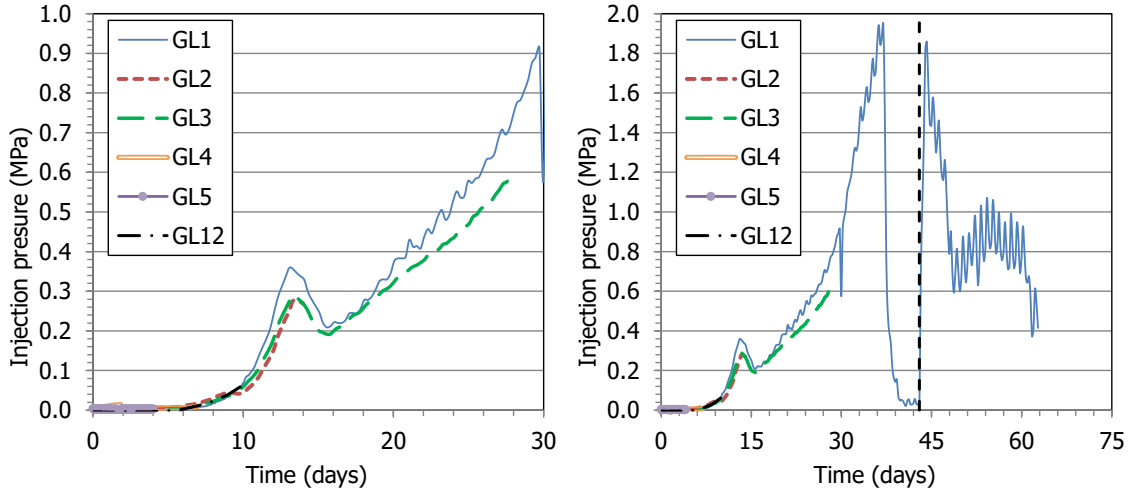

Figure 22. Injection pressure evolution in the GAP-liquid tests (the dotted vertical line indicates the closing of the upper outlet in test GL1 preceded by a blackout)

The evolution of the gap height (which was initially 0.9 cm) and of the bentonite degree of saturation are shown in Figure 23. After about 30 days the gap was completely closed and the samples were fully saturated. Interestingly, the injection pressure started to increase before the gap was completely closed, which highlights that the decrease in permeability occurred irrespective of full swelling having been reached.

Test	Duration (days)	Initial *w* (%)	Initial ρ_d (g/cm^3)	Initial S_r (%)	Initial sample *h* (cm)	Initial gap *h* (cm)	Final *w* (%)	Final ρ_d (g/cm^3)	Final S_r (%)	Final sample *h* (cm)	Final gap *h* (cm)
GL1	63	13.3	1.65	57	2.58	0.83	45.20	1.25	103	3.41	0.00
GL2	14	13.3	1.67	59	2.54	0.87	32.20	1.32	83	3.21	0.20
GL3	28	13.8	1.67	60	2.53	0.90	44.90	1.23	102	3.43	0.00
GL4	7	14.3	1.67	62	2.52	0.89	24.10	1.50	81	2.81	0.60
GL5	4	14.4	1.66	62	2.55	0.85	18.90	1.58	72	2.69	0.70
GL12	10	13.1	1.69	59	2.52	0.90	26.30	1.43	80	2.98	0.44

Table 3. Initial and final characteristics of the GAP-liquid tests with hydration through the bottom

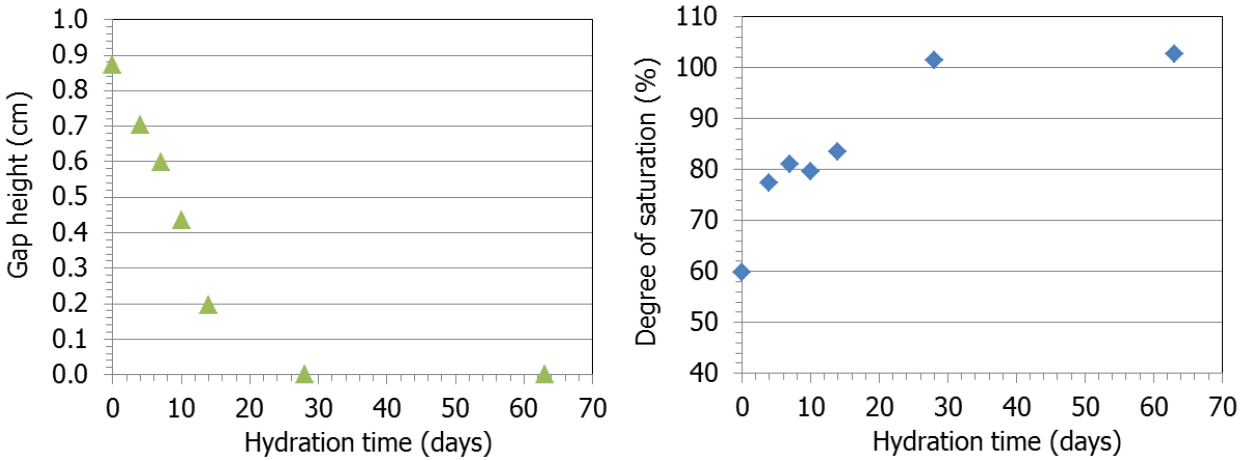

Figure 23. Evolution of gap height and of bentonite degree of saturation in GAP-liquid tests

The water content and dry density at different levels of the samples measured at the end of the tests are shown in Table 4 and plotted in Figure 24. The overall water content increased with time but was always higher towards the hydration surface. In the same way the dry density decreased as the gap was filled and was always lower towards the hydration surface. Although the gradients attenuated over time, they did not disappear, even when the sample was completely saturated: the water content near the hydration surface remained higher and the dry density lower (tests GL1 and GL3).

Test	Duration (days)	Distance (cm)	*w* (%)	ρ_d (g/cm^3)	Distance (cm)	*w* (%)	ρ_d (g/cm^3)	Distance (cm)	*w* (%)	ρ_d (g/cm^3)	Distance (cm)	*w* (%)	ρ_d (g/cm^3)
GL1	63	3.07	43.3	1.25	2.20	43.1	1.23	1.30	45.0	1.22	0.40	49.4	1.17
GL2	14	2.50	25.8	1.36	-	-	-	1.30	30.1	1.30	0.40	40.6	1.24
GL3	28	3.05	42.0	1.21	2.20	42.9	1.21	1.30	44.4	1.19	0.40	50.2	1.15
GL4	7	2.31	19.5	1.53	-	-	-	1.30	22.1	1.50	0.40	30.8	1.42
GL5	4	2.30	15.5	1.60	-	-	-	1.31	17.7	1.58	0.35	23.6	1.52
GL12	10	2.55	22.1	1.44	-	-	-	1.55	24.1	1.47	0.45	32.7	1.39

Table 4. Final water content (w) and dry density (ρ_d) along the samples of GAP-liquid tests (distance from hydration surface)

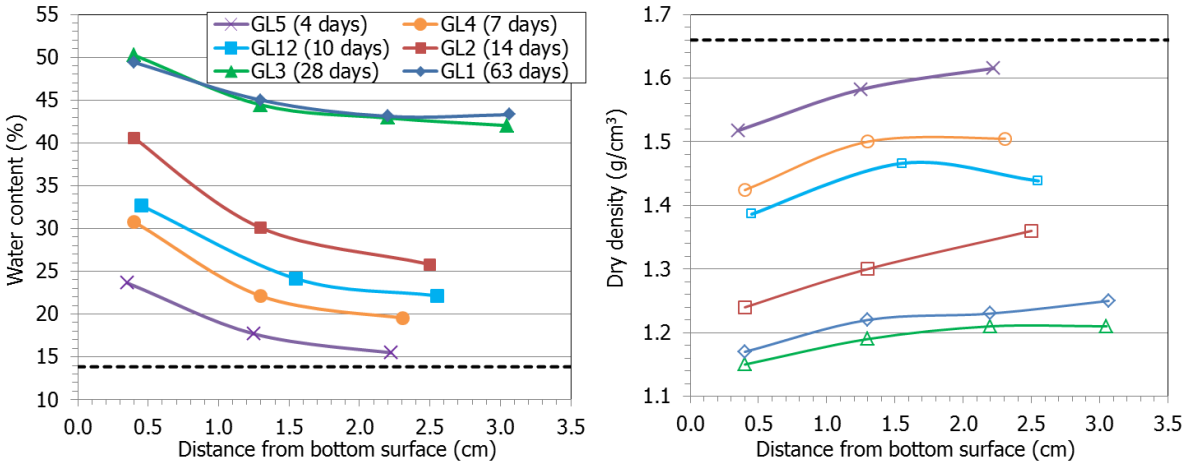

Figure 24. Final water content and dry density of GAP-liquid tests at different levels of samples (the dotted horizontal lines indicate the initial values)

4.2.2 INJECTION FROM GAP

Seven tests in which the bentonite was saturated from the gap (as in the GAP-vapour tests) were performed and dismantled after different hydration times (Table 5). They all had the same nominal initial characteristics. The bottom outlet remained open to atmosphere during the whole duration of the test, except in the longest one (GL13). At the beginning of the tests, a flow rate was prescribed and the gap on top of the cell became initially inundated. During the first test, GL6, it was realised that it was no possible to identify how much water had been actually taken by the bentonite, by the porous stone on top, or had gone between the porous stone and the cell wall. To partly solve this uncertainty, in the rest of the tests the upper porous stone was saturated outside the cell prior to test initiation (which made the samples take some water from it before water injection started). In test GL10 a saturated porous stone was placed in contact with the bentonite sample inside the cell (in the same way as for the other tests), but no water injection took place. After 6 days, the cell was dismantled and the water content along the sample was determined, so that to estimate the water quantity taken by the sample from the porous stone. The average water content of the bentonite increased to 17.8% in one day just by adsorption of the water in the porous stone, and in two days to 18.6%, with a considerable gradient from top to bottom (Figure 25). The right part of this Figure allows to see that the central part of the bentonite sample swelled more. This is why the postmortem subsampling was done considering separately the internal and external parts of each section (Figure 6, right).

Test	Duration (days)	Initial *w* (%)	Initial ρ_d (g/cm^3)	Initial S_r (%)	Initial sample *h* (cm)	Initial gap *h* (cm)	Final *w* (%)	Final ρ_d (g/cm^3)	Initial S_r (%)	Final sample *h* (cm)	Final gap *h* (cm)
GL6	7	14.3	1.66	62	2.55	0.87	29.0	1.22	64	3.42	0.00
GL7[a]	7	14.4	1.67	63	2.54	0.88	33.6	1.22	75	3.42	0.00
GL8[a]	22	14.1	1.67	61	2.56	0.85	45.1	1.25	105	3.41	0.00
GL9[a]	14	13.6	1.70	63	2.53	0.89	41.2	1.26	98	3.41	0.00
GL10[a, b]	6	14.9	1.68	67	2.52	0.89	20.9	1.36	57	3.06	0.35
GL11[a]	2	14.3	1.67	62	2.51	0.91	18.3	1.47	59	2.87	0.78
GL13[a]	39	14.3	1.66	63	2.55	0.87	45.8	1.24	104	3.42	0.00

[a] upper porous stone saturated before starting water injection; [b] no water injection

Table 5. Initial and final characteristics of the GAP-liquid tests with hydration from gap

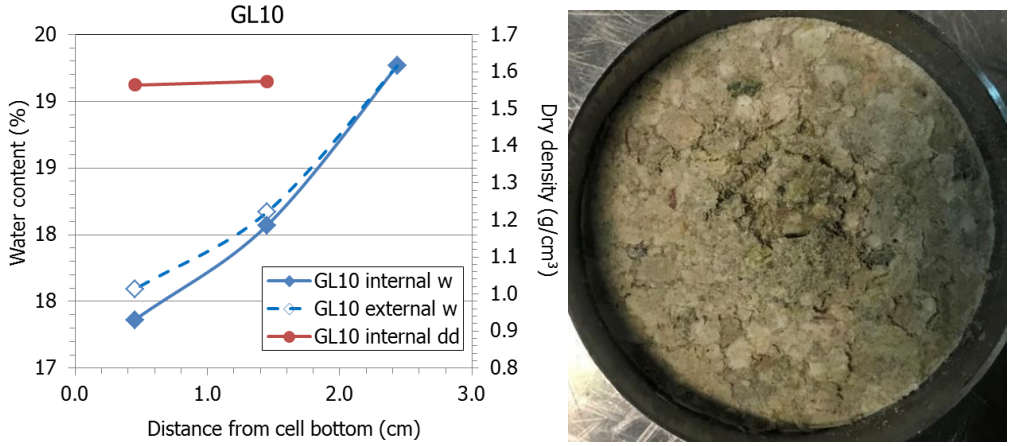

Figure 25. Change in water content and dry density along a bentonite sample in contact with a saturated porous stone for 6 days and final appearance of the top of the sample (hydration from top gap)

In order to keep the flow rate prescribed (0.07 cm^3/h), the injection pressure was null at the beginning of the experiments and started to increase after 11 days from the beginning of injection (Figure 26). The degree of saturation when this happened was between 75 and 87%. The tables with the numerical values of the pressure and water intake along the tests are included in the Annex (Table A- 22 to Table A- 27).

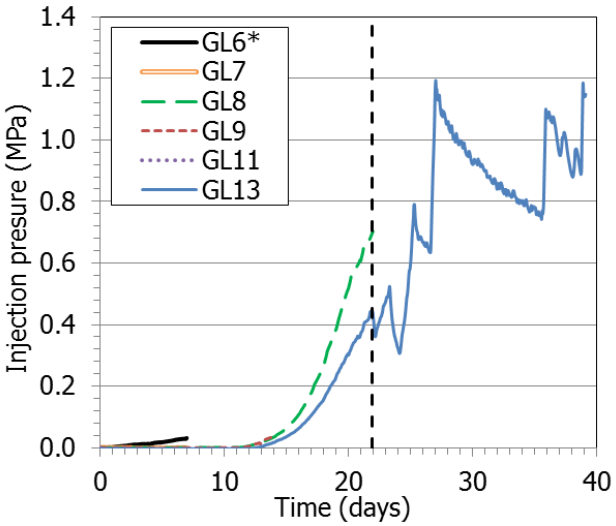

Figure 26. Injection pressure evolution in the GAP-liquid tests with hydration through the gap (the dotted vertical line indicates the closing of the outlet in test GL13)

The evolution of the gap height and of the bentonite degree of saturation are shown in Figure 27. The gap was closed after 7 days. After 22 days the sample was fully saturated (S_r=105%).

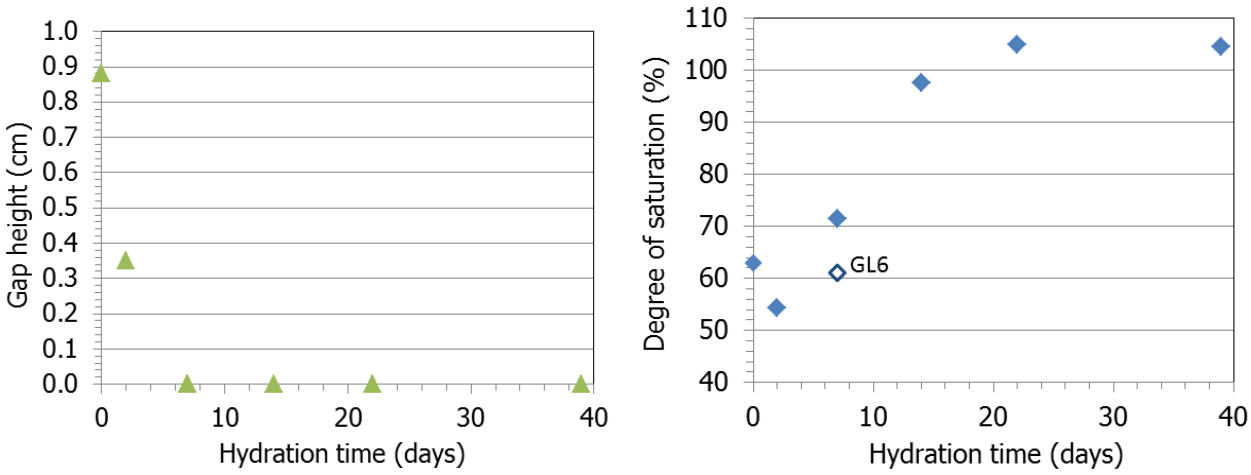

Figure 27. Evolution of gap height and of bentonite degree of saturation in GAP-liquid tests with hydration from gap

The external and internal water content and dry density of the bentonite at different levels along the samples are shown in Table 6 and plotted in Figure 28. The swelling of the bentonite surface close to the gap was irregular in the shorter tests (GL6, GL7, GL11) and the water content of the central area was higher than in the periphery (Figure 29). In contrast, for the longer tests the water content along the whole sample was higher in the external part of each section than in the internal part. The comparison of the two longer tests (GL8 and GL13) shows that although after 22 days (test GL8) the sample was virtually saturated, the water content and dry density distributions along the sample differed with respect to those after 39 days (test GL13): the water content close to the gap had reached its higher value, but had not equilibrated yet farther away from the gap. As well, the dry density close to the gap decreased from 22 to 39 days of hydration.

Test	Distance (cm)	w (%)		ρ_d (g/cm^3)		Distance (cm)	w (%)		ρ_d (g/cm^3)		Distance (cm)	w (%)		ρ_d (g/cm^3)	
		Internal	External	Internal	External		Internal	External	Internal	External		Internal	External	Internal	External
GL6[a]	2.78	48.0	-	-	-	1.65	23.2	24.8	-	-	0.55	20.8	20.4	1.53	-
GL7	2.77	52.0	46.1	-	-	1.65	29.9	27.4	-	-	0.55	23.1	22.2	1.49	-
GL8	3.05	50.8	53.9	0.87	0.99	1.30	41.9	42.9	1.19	1.19	0.40	40.0	40.2	1.24	1.26
GL9	2.78	48.6	49.5	1.14	1.1	1.65	40.4	40.6	1.19	1.20	0.55	33.9	34.6	1.31	1.32
GL10[b]	2.43	19.3	19.3	-	-	1.45	18.1	18.2	1.57	-	0.45	16.5	16.4	1.59	-
GL11	2.63	26.8	26.8	-	-	1.60	19.0	19.9	1.52	1.56	0.50	16.5	16.4	1.61	-
GL13	3.06	51.1	53.2	1.06	1.05	1.30	42.8	42.4	1.22	1.13	0.40	42.7	41.0	1.20	1.19

[a] upper porous stone initially dry; [b] no hydration

Table 6. Internal and external final water content (w) and dry density (ρ_d) along the samples of GAP-liquid tests with hydration from gap (distance from bottom surface)

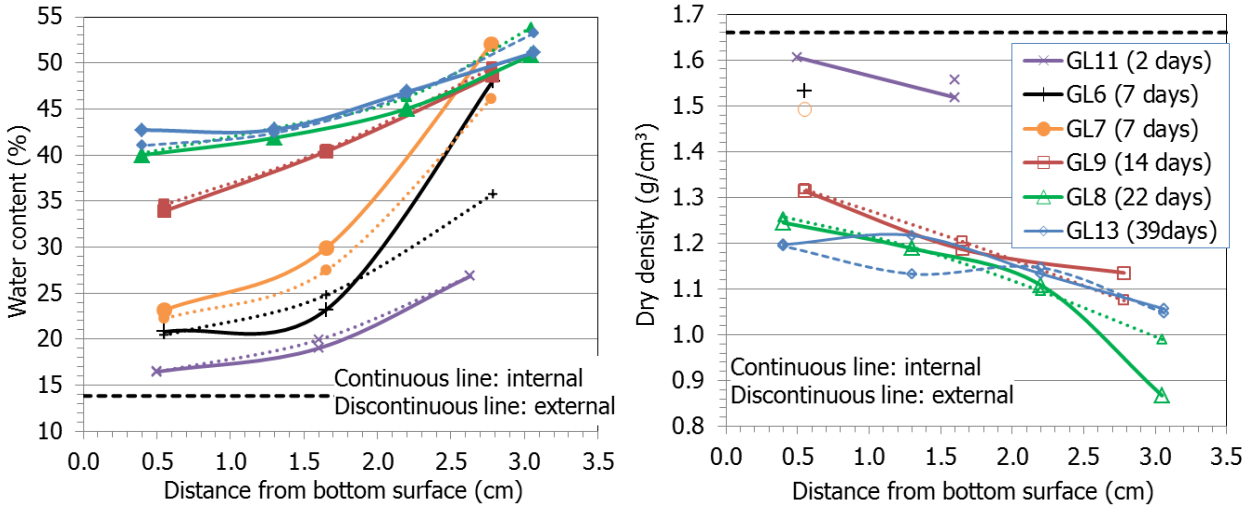

Figure 28. Final water content and dry density of GAP-liquid tests with hydration from gap at different levels of samples (hydration from top gap). The dotted horizontal lines indicate the initial values

Figure 29. Final appearance (upper and lateral views) of sample GL7 (7 days)

4.2.3 COMPARISON

In this section, the two different types of GAP-liquid test (hydration from bottom surface and from gap surface) are compared. When hydration took place from the gap, it was faster than the hydration from the opposite surface, as attested by the evolution of water content (Figure 30). Consequently the dry density also decreased initially faster and reached earlier the lowest possible value when the bentonite was hydrated from the gap. As a result, the gap closed sooner when hydration occurred from the gap surface (Figure 31).

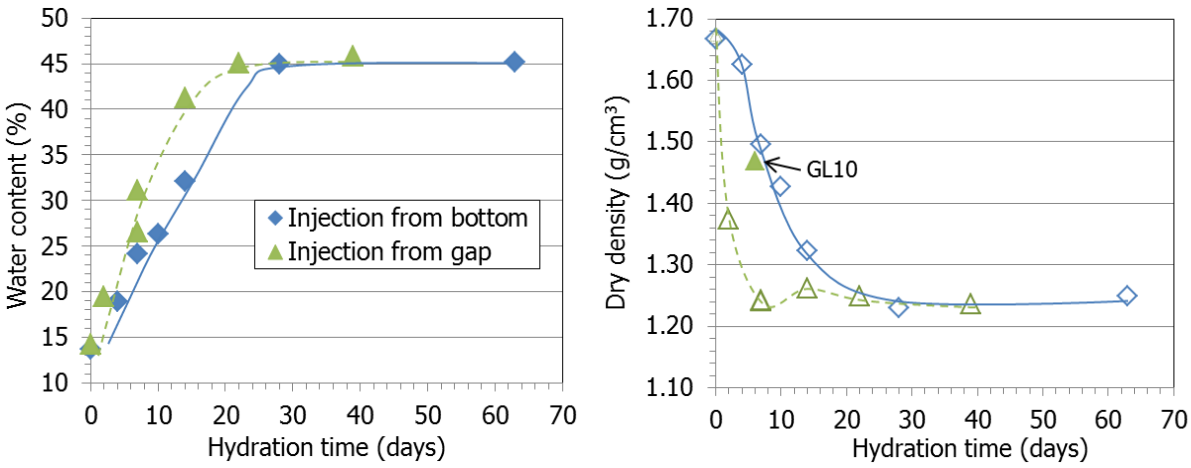

Figure 30. Evolution of water content and dry density in GAP-liquid tests

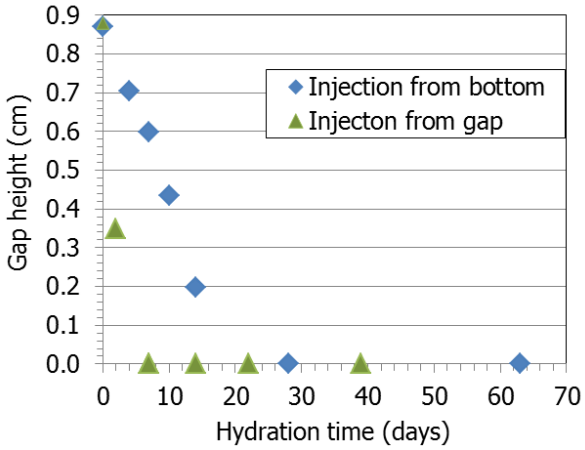

Figure 31. Evolution of gap height in GAP-liquid tests

Figure 32 shows a comparison of the final water content and dry density distribution along the height of the samples from all the tests. The values are plotted as a function of the distance from the hydration surface, which was the bottom of the cell in the tests with saturation opposite to the gap, and the top of the cell in the cells with saturation through the gap (in both cases considering also the thickness of the porous filter). In this case, the water content values for the tests performed with saturation through the gap, are the weighted average values of those measured in the external and internal parts of each section which were plotted in Figure 28. For a given test duration the water content was higher and the dry density lower in the samples saturated through the gap, as the overall values plotted in Figure 30 also showed. As well, the water content and the dry density gradients for tests of similar duration tended to be higher in the samples saturated through the gap, i.e. the water distributed more homogeneously along the sample when hydration took place opposite to the gap, because the process was slower.

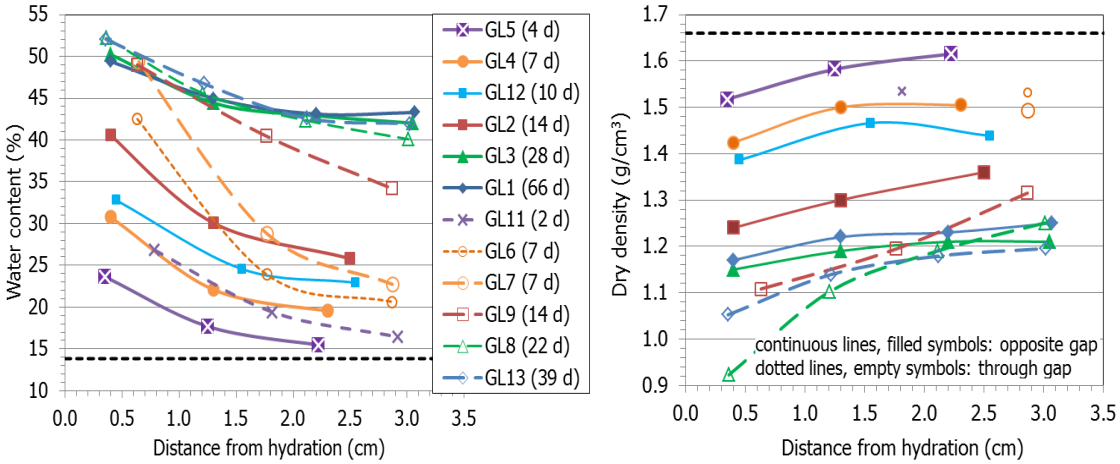

Figure 32. Final water content and dry density along the samples used for GAP-liquid tests (the dotted horizontal lines indicate the initial values)

4.2.4 PORE SIZE DISTRIBUTION

The same analysis of the final pore size distribution of the subsamples described for the GAP-vapour tests was performed with the subsamples of the GAP-liquid tests. The detailed results and the incremental mercury intrusion curves for all the samples are shown in the Annex (Table A- 28, Table A- 29, Figure A- 4, Figure A- 5). As an example for the tests saturated from the bottom, Figure 33 shows the incremental curves of mercury intrusion for the subsamples of the tests lasting 14 and 66 days and for a FEBEX sample compacted with approximately the same dry density and water content as the initial conditions used in the cells (1.69 g/cm^3, 13.5%). In some tests it was not possible to get material from the upper part of the specimens (the one swelling into the void) for the MIP tests because of its inconsistency. In fact, in the tests saturated from the gap the pore size distribution was only obtained for samples of tests GL9, GL11 and GL13 (Figure 34) for lack of enough material. Again, two pore families corresponding approximately to pores larger and smaller than 200 nm could be told apart. The volume of pores larger than 200 nm increased during testing, particularly closer to the gap and as the test was longer. As well, the size of the macropores increased all along the samples and for all testing times (Figure A- 6), whereas the size of the mesopores remained in the range between 5 and 20 nm.

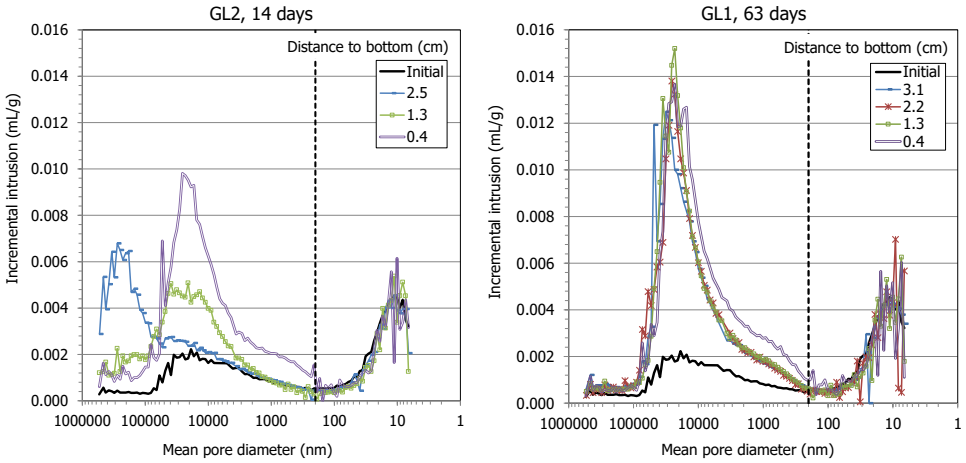

Figure 33. Pore size distribution of samples tested in GAP-liquid cells for 14 days (GL2) and 66 days (GL1) and for the initial block expressed as incremental mercury intrusion (water injection from bottom, opposite to gap)

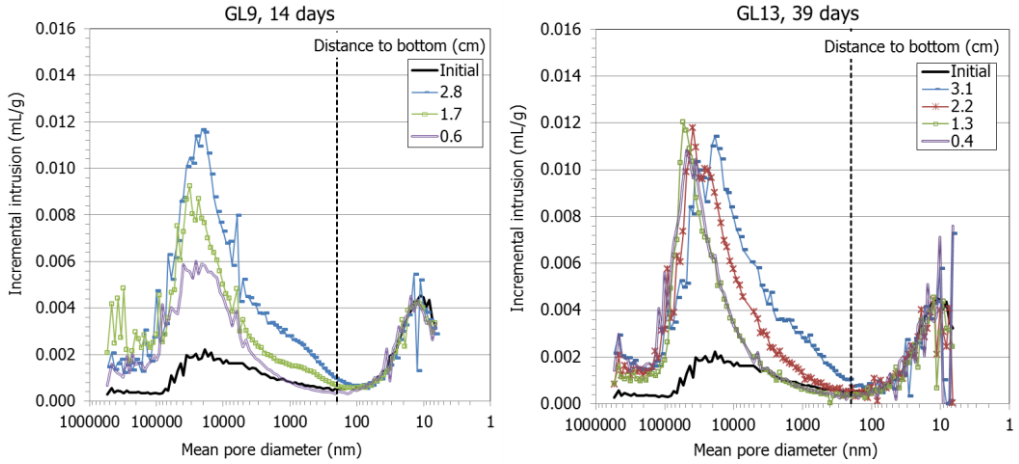

Figure 34. Pore size distribution of samples tested in GAP-liquid cells for 14 days (GL9) and 39 days (GL13) and for the initial block expressed as incremental mercury intrusion (hydration from top gap)

The percentage of pores intruded by mercury in these subsamples was between 28 and 85%. As it was explained for the GAP-vapour tests, in some subsamples (those closest to the gap), part of the porosity not explored by the porosimeter may correspond to pores larger than 550 µm. This would be the case of the upper subsamples of the tests shown in Figure 35, i.e. those shorter than 14 days in the samples saturated from the bottom and shorter than 7 days in the samples saturated from the gap. Taking this into account, the void ratio corresponding to pores larger and smaller than 200 nm was calculated and is plotted in Figure 36 for the tests saturated from the bottom and in Figure 37 for the tests saturated from the gap. Although the volume of pores smaller than 200 nm was initially higher, over time the volume of macropores increased more, and in fact the two longer tests had the highest void ratio corresponding to macropores, irrespective of the way of hydration. As a result, the ratio between the void ratios corresponding to pores smaller (e_m) and larger (e_M) than 200 nm significantly decreased during testing for the longer tests and was lower for the subsamples closer to the gap, where the bentonite could freely swell. It is remarkable that, in the tests with hydration through the bottom, this ratio was the same after 28 and 63 days,

possibly indicating steady conditions, which were also shown by the water content and dry density distributions (Figure 24).

There are only available results for three tests with hydration from the gap (Figure 37). After 2 days only the subsample closest to the hydration surface experienced a huge increase in the size of the macropores. After 14 days the volume of macropores increased considerably with respect to the original sample in all subsamples, but more as the subsample was closer to the gap. This resulted in an overall decrease in e_m/e_M ratio.

Figure 35. Appearance upon dismantling of some of the shorter GAP-liquid tests (hydration from bottom or gap)

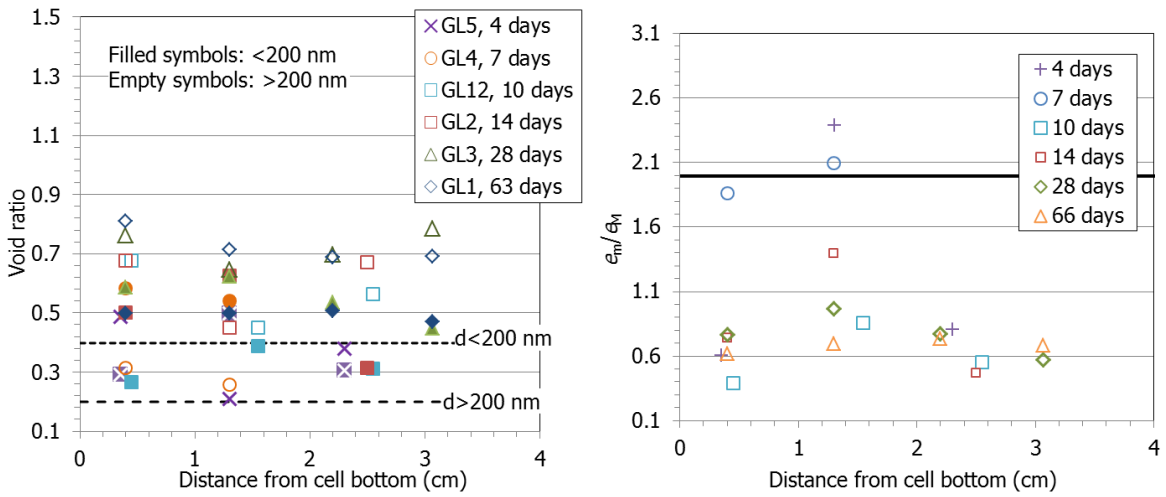

Figure 36. Void ratio corresponding to pores smaller (e_m) and larger than 200 nm (e_M) obtained by MIP in samples tested in GAP-liquid cells saturated from the opposite surface to the gap for different times (left) and ratio between both (right). The thick horizontal lines indicate the values for the initial block

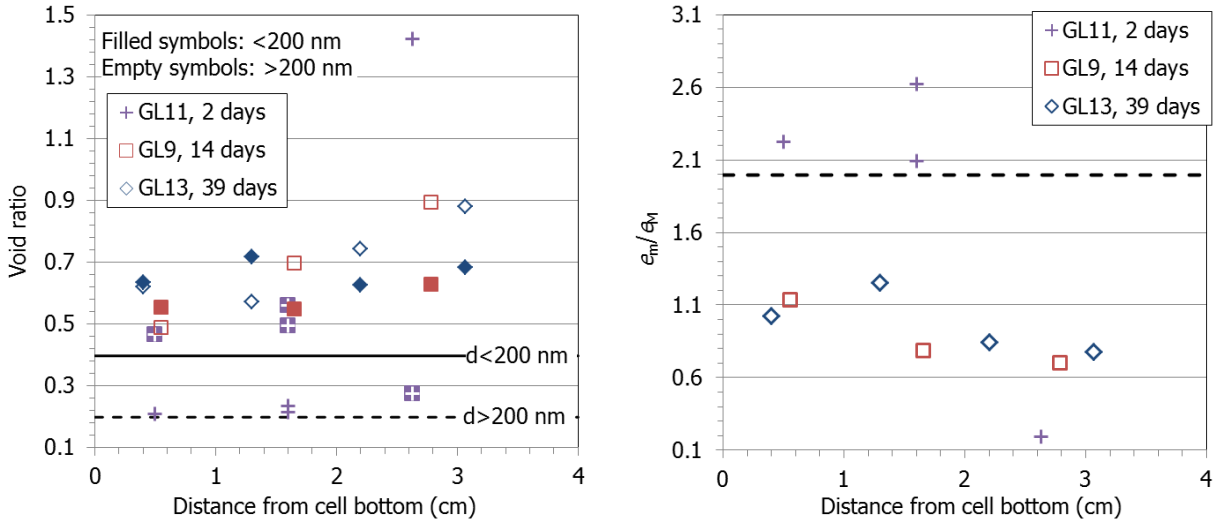

Figure 37. Void ratio corresponding to pores smaller (e_m) and larger than 200 nm (e_M) obtained by MIP in samples tested in GAP-liquid cells saturated from the gap for different times (left) and ratio between both (right). The thick horizontal lines indicate the values for the initial block

The evolution over time of the void ratio corresponding to different pore sizes is shown in Figure 38 for the different subsamples. This representation allows to see that the changes are quicker and more drastic when hydration takes place through the gap; that the samples saturated through the bottom experienced very soon an overall increase in macropore (and micropore) void ratio at all locations; and that a "steady microstructural state" was reached after 30 days (for the samples saturated through the bottom). Maybe the main difference between the samples saturated through the gap or opposite to it in terms of microstructural evolution was that in the first case the increase of void ratio affected all pore sizes, whereas in the samples saturated opposite to the gap the macropores experienced the major increase in void ratio.

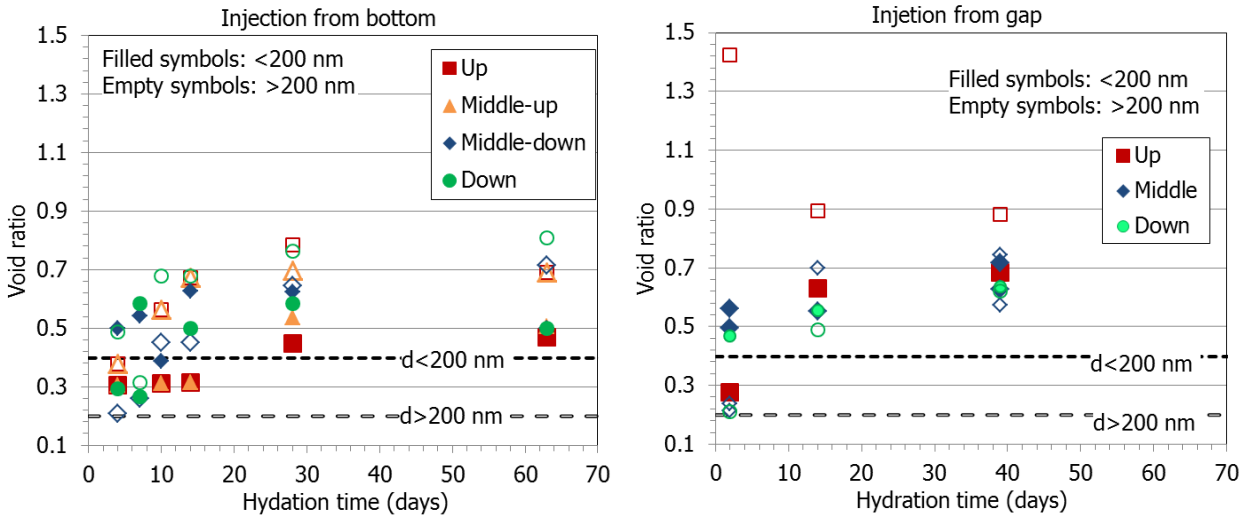

Figure 38. Evolution of void ratio over time corresponding to pores larger and smaller than 200 nm for the two sets of GAP-liquid tests. The dotted horizontal lines indicate the values for the initial sample (time=0)

5 DISCUSSION

The evaluation of the results obtained in the two kinds of cells indicates that hydration was slower via water vapour than liquid water and that the hydration kinetics was also affected by the actual suction and by the position of the gap with respect to the hydration source (Figure 39). The final water content of the samples saturated via vapour transfer was approximately related to the water retention curve (Figure 10). Thus, the final swelling of the samples under suction 6 MPa was not enough as to close the gap, which would have meant a 20% swelling. The samples saturated under the lowest suction (0.5 MPa) were able to swell enough as to close the gap before the equilibrium water content had been reached. These samples could have taken more water if swelling had been allowed (Figure 8). Indeed under a given vertical stress (null in the case of the GAP tests) the swelling capacity increases with the decrease in suction.

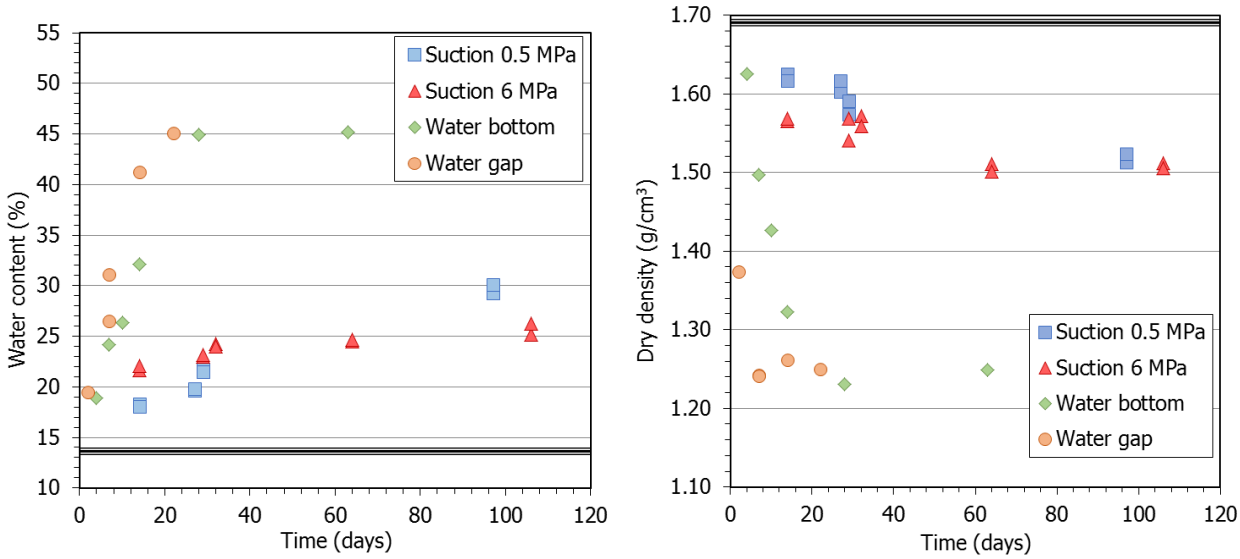

Figure 39. Evolution of water content and dry density in all tests. The thick horizontal lines indicate the initial values

However in the GAP-vapour tests the final overall water contents were lower and the dry densities higher than in the GAP-liquid tests, because the void height was larger in the latter (9 mm vs. 5 mm, corresponding to a potential swelling of 32 vs. 20%). As a result of the higher dry density of the GAP-vapour tests, and despite their lower water content, the final degree of saturation of the tests performed under suction 0.5 MPa was in the order of the GAP-liquid tests (Figure 40).

The velocity of saturation was also different in the two kinds of tests performed with liquid water, even though the flow rate prescribed was the same in the two sets of tests. When water was supplied through the gap, the samples saturated more quickly because they were able to swell into the open void and take water immediately (because of the higher permeability of the swollen, low-density bentonite), developing higher internal dry density and water content gradients. Saturation was slower when it took place from the opposite side to the gap, where no free swelling was readily allowed and the permeability of the bentonite was lower because its dry density was higher (see relation between dry density and hydraulic conductivity in Equations [2]

and [3]). Consequently the overall block dry density also decreased initially faster and reached earlier the lowest possible value when the bentonite was hydrated from the gap, which closed sooner. For similar test durations the dry density close to the hydration surface of the tests saturated through the bottom was higher than that of the tests saturated through the gap (Figure 41), which would explain that water pressure developed earlier in the former (Figure 42).

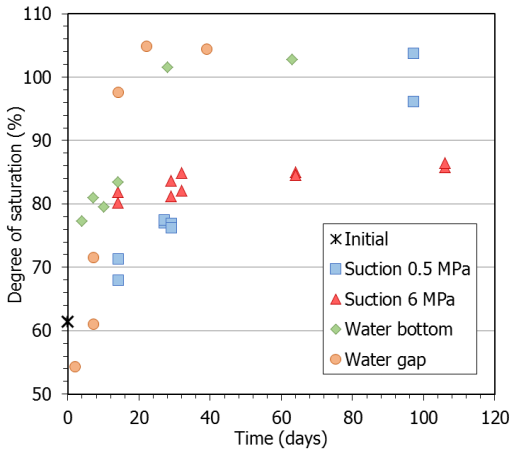

Figure 40. Evolution of the degree of saturation in tests shorter than 100 days

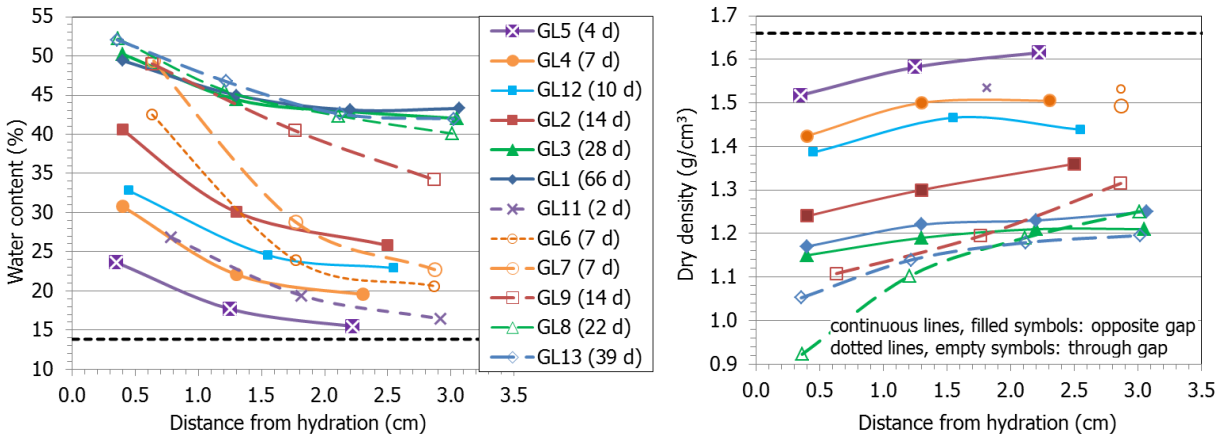

Figure 41. Final water content and dry density along the samples used for GAP-liquid tests. The dotted horizontal lines indicate the values for the initial sample (time=0)

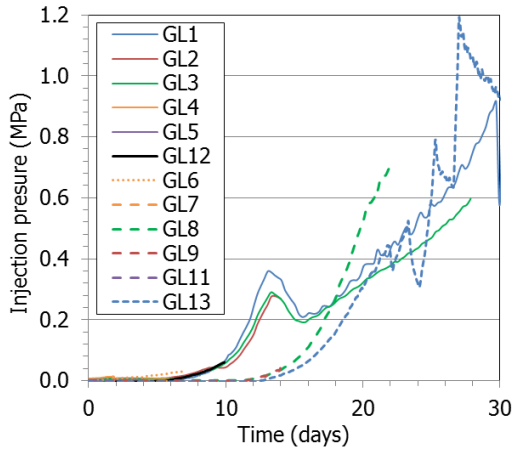

Figure 42. Injection pressure evolution in the GAP-liquid tests with saturation from the bottom (continuous lines) and from the gap (dotted lines). In test GL1 the injection pressure increased up to 2 MPa and the upper outlet was closed because water was flowing out (not shown in the Figure)

In turn, the faster the hydration the larger the strains initially occurred and their irreversibility. As a result, the persistence of water content and dry density gradients was linked to the velocity of saturation: the quicker the hydration took place, the steeper and more persistent the gradients were. Hence the gradients were more remarkable and persistent when hydration took place in the water phase, then under "high" suction and finally under low suction. In tests sufficiently long steady gradients were reached, with no further changes in water content or dry density. Figure 43 illustrates these observations by comparing the results in terms of water content and dry density for tests of different kinds long enough as to have reached steady conditions. Indeed the time needed to reach "steady conditions" was much longer in the GAP-vapour tests. Note that the minimum possible overall dry density and maximum water content of the GAP-vapour tests were ~1.42 g/cm^3 and ~35%, and for the GAP-liquid tests ~1.25 g/cm^3 and ~44%, because of the different gap dimensions. Nevertheless, no completely homogeneous density or water content distribution was observed in any of the tests, and the bentonite that was closer to the gap had final higher water content and lower dry density.

Because of the swelling into the gap, hydration brought about an overall increase in the void ratio corresponding to all pore sizes. Although the volume of pores smaller than 200 nm was initially higher, over time the volume of macropores increased more than that of smaller pores (Figure 20, Figure 38), giving place to an overall decrease of the ratio between the void ratio corresponding to pores smaller (e_m) and larger (e_M) than 200 nm, which also tended to be constant along the sample in the longer tests (Figure 44).

The increases in macropore void ratio were much more notable in the samples saturated with liquid water, which can be related to the lower dry densities that they reached. In agreement with the different hydration kinetics of the different kinds of tests, the overall macropore void ratio increase took place very quickly in the samples saturated with liquid water, particularly in the subsamples closest to the gap (Figure 45). Besides, in the samples saturated with liquid water through the gap the increase of void ratio affected all pore sizes, whereas in the samples saturated opposite to the gap it was the macropores that experienced the largest increase in void ratio, resulting in final lower e_m/e_M ratios. In the samples tested under suction, the macropore void ratio increase was also quick close to the gap, but took longer in positions away from it. The size of the macropores increased as well, but in the GAP-vapour tests the increase was more notable in the shorter ones and later the size of macropores decreased to values which were still higher than the initial one, the same trends being observed all along the samples. In contrast, the macropore size in the GAP-liquid tests increased more away from the hydration surface. The changes in void ratio corresponding to pores smaller than 200 nm were overall more uniform across the samples, although in the samples saturated with liquid water e_m increased more close to the gap.

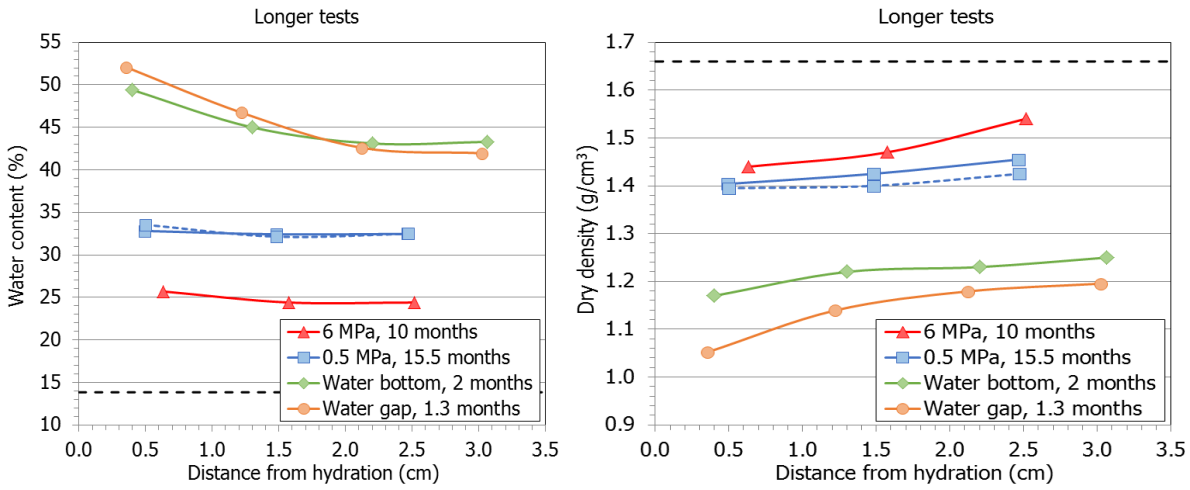

Figure 43. Final water content and dry density of subsamples of all tests long enough as to have reached steady conditions. Hydration from gap in all cases except in the "Water bottom" series. The dotted horizontal lines indicate the values for the initial sample (time=0)

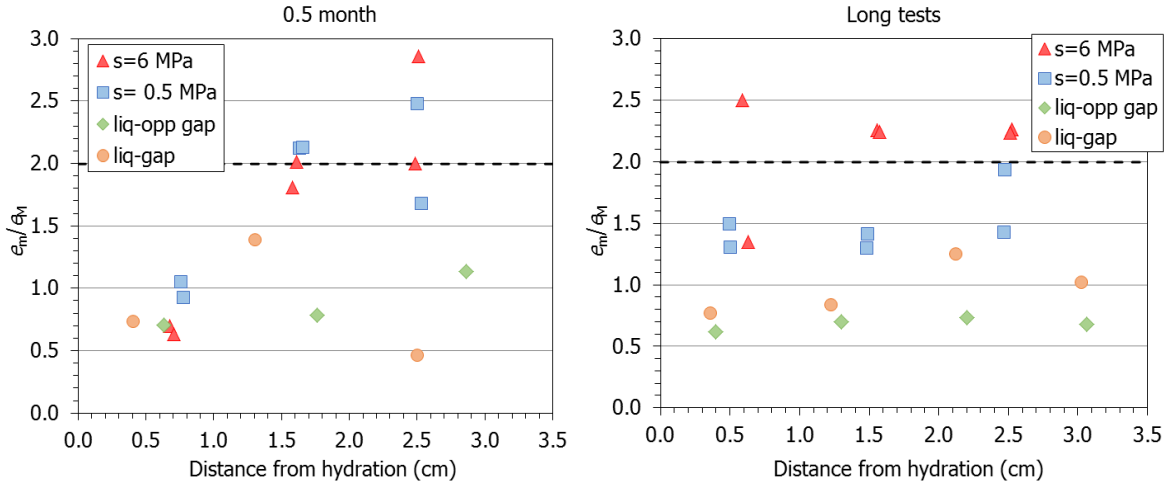

Figure 44. Ratio between void ratio corresponding to pores smaller and larger than 200 nm in tests of duration 0.5 month (left) and tests having reached steady conditions (right, same as in Figure 43). The dotted horizontal lines indicate the values for the initial sample (time=0)

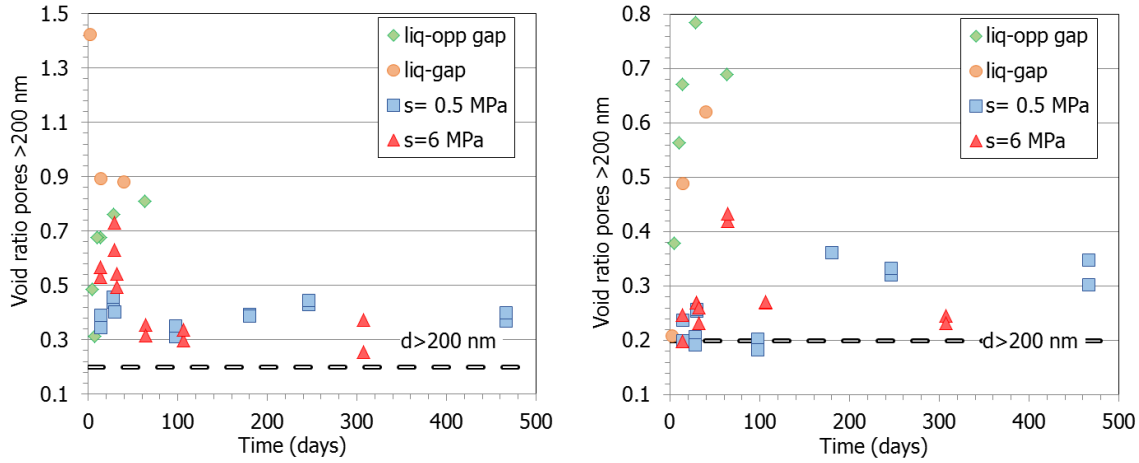

Figure 45. Void ratio corresponding to pores >200 nm for the subsamples closest to hydration (left) and opposite to hydration (right) for the GAP-liquid and GAP-vapour tests. The dotted horizontal lines indicate the values for the initial sample

As a result of these changes, the e_m/e_M ratio was lower in the subsamples closest to the gap in the shorter tests, but in longer tests tended to be the same in all the bentonite block, and lower than the initial one, which would be an additional indication of equilibrium being reached (Figure 44). Only in the tests performed under suction 6 MPa, in which the gap was not closed because of the lower equilibrium water content, the final e_m/e_M ratio was higher than the initial one.

Hydration of bentonite samples under confined conditions has been usually reported to result in an increase of micropore void ratio and a homogenization of the pore sizes towards smaller values (Villar et al. 2017). This observation is in contrast with the results reported here, where a general increase of the macropore void ratio and of the macropore mode size was observed, which may indicate that the presence of a gap where the bentonite swelled into really affected the kind of microstructural changes.

6 CONCLUSIONS

In the context of the deep geological disposal of nuclear waste and to improve the understanding of the homogenization process of bentonite barriers, in particular with regards to the filling of technological voids, a series of tests were performed in compacted FEBEX bentonite cylindrical samples hydrated under limited axial swelling conditions, i.e. with a gap on top. These samples were hydrated with water in vapour (GAP-vapour) or liquid phase (GAP-liquid). From the observations and analysis reported, the following conclusions can be drawn:

- The final water content of the samples saturated via vapour transfer was approximately related to the water retention curve, although with equilibrium values slightly above those expected for bentonite of similar dry densities subjected to the same suctions under confined conditions. Indeed the final swelling strain is related to the final water content, and if this is too low, swelling might not be enough as to close the gap, as it happened in the tests under suction 6 MPa. Hence, in a real repository case, if the relative humidity is low (suction is high), technological voids might not be filled.

- Hydration was slower via water vapour than liquid water, but the hydration kinetics was also affected by the actual suction and by the boundary conditions (it was faster through the gap than through the opposite side). When liquid water was supplied through the gap, the samples saturated more quickly because they were able to swell into the open void, where the bentonite density was initially very low and its permeability higher, allowing a fast initial water intake. As the water content increased, the overall dry density decreased and the size of the gap reduced. The gap would close faster the quicker the hydration.

- At the end of the tests the bentonite water content was higher close to the hydration surface and its dry density lower. The faster the hydration the larger the strains initially occurred and their irreversibility. Hence, the quicker the hydration took place, the steeper and more persistent the gradients were. In tests sufficiently long no further changes in water content or dry density were observed, even though no completely homogeneous density or water content spatial distribution was reached.

- Because of the swelling into the gap the samples experienced an overall increase in the void ratio corresponding to all pore sizes, but the microstructural changes were quicker and more drastic when hydration was faster. Although the volume of pores smaller than 200 nm (void ratio e_m) was initially higher, over time the volume of macropores (void ratio e_M) increased more than that of smaller pores, and faster in the samples closer to the gap and in those saturated with liquid water, giving place to an overall decrease of the e_m/e_M ratio, which also tended to be constant along the sample in the longer tests. Only in the tests performed under suction 6 MPa, in which the gap was not closed because of the lower equilibrium water content, the final e_m/e_M ratio was higher than the initial one. The size of the macropores significantly increased in the first stages, but tended to decrease over time, likely in connection with the closing of the gap.

Overall, the results reported in this paper are consistent with the key features of behaviour underlying the homogenization processes, which according to the modelling work performed in the framework of the BEACON project would be stress path dependency and strain irreversibility (Gens 2021). However, the patterns described in the two last bullets cannot be extrapolated to the bulk of the barrier, since they have been obtained in tests representing the areas closest to the technological voids.

With a view on future research, it must be highlighted that all the tests were performed with the same initial dry density, and that since the initial swelling seems to considerably affect the "long-term" evolution, samples with different initial dry density –or of different bentonites–, and consequently, swelling potential, may behave differently. Also the size of the gap, and consequently the minimum density that the samples may reach, is a factor that could affect the irreversibility of the strains and gradients observed. This might have played a role in the differences observed between the GAP-liquid and the GAP-vapour tests. For the samples saturated in the water phase, the effect of water injection pressure should also be checked.

7 REFERENCES

[1] ENRESA 2006. FEBEX Full-scale Engineered Barriers Experiment, Updated Final Report 1994-2004. Publicación Técnica ENRESA 05-0/2006, Madrid, 590 pp

[2] García-Siñeriz, J.L., Villar, M.V., Rey, M., Palacios, B., 2015. Engineered barrier of bentonite pellets and compacted blocks: state after reaching saturation. Engineering Geology 192, 33–45. https://doi.org/10.1016/j.enggeo.2015.04.002

[3] Gens, A. 2021. Description of the constitutive models developed in the project. Conceptual bases, mathematical description and model capabilities. Assessment of predictive power. BEACON Deliverable D3.3. 338 pp. https://www.beacon-h2020.eu/deliverables/

[4] Sánchez M, Gens A, Guimarães L, Olivella S, 2005. A double structure generalized plasticity model for expansive materials. International Journal for Numerical and Analytical Methods in Geomechanics 29: 751–787. DOI:10.1002/nag.434.

[5] Sing, K.S.W., Everett, D.H., Haul, R.A.W., Moscou, L., Pierotti, R.A., Rouquérol, J., Siemieniewska, T. 1985. Reporting physisorption data for gas/solid systems with special reference to the determination of surface area and porosity. Pure and Applied Chemistry 57(4): 603-619. IUPAC.

[6] Villar, M.V. 2002. Thermo-hydro-mechanical characterisation of a bentonite from Cabo de Gata. A study applied to the use of bentonite as sealing material in high level radioactive waste repositories. Publicación Técnica ENRESA 01/2002, Madrid, 258 pp.

[7] Villar MV, 2007. Water retention of two natural compacted bentonites. Clays and Clay Minerals 55(3): 311-322.

[8] Villar, M.V.(Ed). 2017. FEBEX-DP Postmortem THM/THC Analysis Report. NAB 16-017. 143 pp.

[9] Villar MV, Gómez-Espina R, Gutiérrez-Nebot L, 2012. Basal spacings of compacted bentonite. Applied Clay Science 65-66: 95-105.

[10] Villar, M.V., Campos, G., Gutiérrez-Nebot, L., Arroyo, X. 2019. Effect of prolonged drying at high temperature on the water retention capacity of bentonite (FEBEX-DP samples). Applied Clay Science 182: 105290. https://doi.org/10.1016/j.clay.2019.105290

[11] Villar, M.V., Iglesias, R.J., García-Siñeriz, J.L., Lloret, A., Huertas, F. 2020. Physical evolution of a bentonite buffer during 18 years of heating and hydration. Engineering Geology 264: 105408. https://doi.org/10.1016/j.enggeo.2019.105408

[12] Villar, M.V., Iglesias, R.J., Gutiérrez-Álvarez, C., Carbonell, B. 2021. Pellets/block bentonite barriers: laboratory study of their evolution upon hydration. Engineering Geology 106272. https://doi.org/10.1016/j.enggeo.2021.106272

[13] Villar, M.V., Gutiérrez-Álvarez, C., Campos, G. 2022. Bentonite swelling into a void under suction and water flow. Acta Geotechnica.

[14] Yuan, S., Liu, X., Romero, E., Delage, P., Buzzi, O. 2020. Discussion on the separation of macropores and micropores in a compacted expansive clay. Géotechnique Letters 10: 1–7. https://doi.org/10.1680/jgele.20.00056

ANNEX: DETAIL OF GAP TESTS RESULTS

GAP VAPOUR TESTS RESULTS UNDER SUCTION 6 MPa

Table A- 1. Results of duplicate tests (initial ρd=1.7 g/cm3, initial w=14%, initial h=2.5 cm) under s=6 MPa of duration 14 days

Sample	Time (days)	*w* (%)	ρ_d (g/cm^3)	h (cm)	$\Delta h/h_o$ (%)	S_r (%)
9	0	13.5	1.72	2.478	0.0	64
9	7	17.5	1.64	2.595	4.7	73
9	14	21.6	1.57	2.715	9.6	81
10	0	13.5	1.72	2.473	0.0	64
10	7	18.5	1.63	2.602	5.2	77
10	14	22.1	1.57	2.710	9.6	83

Table A- 2. Results of tests (initial ρ_d=1.7 g/cm^3, initial w=14%, initial h=2.5 cm) under s=6 MPa of duration 1 month

Sample	Time (days)	*w* (%)	ρ_d (g/cm^3)	h (cm)	$\Delta h/h_o$ (%)	S_r (%)
3	0	14.2	1.71	2.489	0.0	66
3	14	20.9	1.60	2.649	6.4	83
3	29	23.0	1.57	2.710	8.9	86
4	0	14.2	1.70	2.494	0.0	66
4	14	20.7	1.58	2.692	7.9	78
4	29	23.1	1.54	2.758	10.6	83
11	0	13.5	1.74	2.434	0.0	67
11	12	20.4	1.60	2.651	8.9	81
11	32	24.3	1.57	2.703	11.0	91
12	0	13.5	1.73	2.447	0.0	66
12	12	21.3	1.61	2.642	8.0	85
12	32	24.0	1.56	2.723	11.3	89

Table A- 3. Results of duplicate tests (initial ρ_d=1.7 g/cm^3, initial w=14%, initial h=2.5 cm) under s=6 MPa of duration 2 months

Sample	Time (days)	*w* (%)	ρ_d (g/cm^3)	h (cm)	$\Delta h/h_o$ (%)	S_r (%)
1	0	14.2	1.70	2.493	0.0	66
1	14	21.4	1.59	2.668	7.0	83
1	29	23.5	1.54	2.766	10.9	84
1	43	24.9	1.51	2.816	12.9	85
1	57	25.0	1.51	2.813	12.8	86
1	64	24.5	1.51	2.813	12.8	84
2	0	14.2	1.71	2.491	0.0	66
2	14	22.1	1.56	2.718	9.1	82
2	29	24.0	1.53	2.781	11.6	84
2	43	24.8	1.51	2.820	13.2	84
2	57	25.1	1.50	2.824	13.4	85
2	64	24.7	1.50	2.831	13.7	83

Table A- 4. Results of duplicate tests (initial ρ_d=1.7 g/cm^3, initial w=14%, initial h=2.5 cm) under s=6 MPa of duration 3.5 months

Sample	Time (days)	*w* (%)	ρ_d (g/cm^3)	h (cm)	$\Delta h/h_o$ (%)	S_r (%)
6	0	14.2	1.71	2.493	0.0	66
6	14	22.5	1.56	2.732	9.6	83
6	28	24.8	1.52	2.791	12.0	87
6	43	24.9	1.52	2.796	12.1	87
6	62	24.6	1.52	2.788	11.8	86
6	76	24.9	1.50	2.826	13.3	85
6	91	25.1	1.51	2.820	13.1	86
6	106	25.1	1.51	2.812	12.8	86
7	0	14.2	1.70	2.494	0.0	66
7	14	22.8	1.55	2.749	10.2	83
7	28	25.1	1.52	2.792	11.9	87
7	43	24.5	1.52	2.796	12.1	85
7	62	25.1	1.52	2.797	12.1	87
7	76	25.7	1.50	2.828	13.4	87
7	91	25.8	1.51	2.808	12.6	89
7	106	26.2	1.51	2.822	13.2	89

Table A- 5. Results of duplicate tests (initial ρ_d=1.7 g/cm^3, initial w=14%, initial h=2.5 cm) under s=6 MPa of duration 10 months

Sample	Time (days)	*w* (%)	ρ_d (g/cm^3)	h (cm)	$\Delta h/h_o$ (%)	S_r (%)
5	0	14.2	1.68	2.535	0.0	63
5	14	22.0	1.57	2.714	7.1	82
5	28	24.1	1.49	2.850	12.4	80
5	43	23.7	1.49	2.849	12.4	79
5	62	24.7	1.48	2.871	13.3	81
5	76	24.4	1.47	2.897	14.3	78
5	91	25.0	1.47	2.893	14.1	81
5	106	25.1	1.47	2.901	14.4	80
5	119	24.8	1.46	2.908	14.7	79
5	139	25.1	1.46	2.907	14.7	80
5	154	25.2	1.46	2.907	14.7	80
5	168	25.4	1.45	2.938	15.9	79
5	181	25.2	1.44	2.958	16.7	77
5	195	25.2	1.44	2.947	16.2	78
5	217	25.4	1.45	2.924	15.4	80
5	237	26.2	1.47	2.900	14.4	84
5	247	26.8	1.44	2.950	16.4	83
5	273	26.9	1.46	2.910	14.8	86
5	286	27.0	1.46	2.917	15.1	85
5	307	27.1	1.46	2.907	14.7	86
8	0	14.2	1.71	2.492	0.0	66
8	14	22.0	1.57	2.703	8.5	83
8	28	25.1	1.51	2.808	12.7	86
8	43	25.2	1.51	2.819	13.1	86
8	62	25.4	1.51	2.816	13.0	87
8	76	25.0	1.51	2.817	13.1	85
8	91	25.4	1.51	2.808	12.7	87
8	106	25.5	1.50	2.827	13.5	86
8	119	25.5	1.52	2.805	12.5	88
8	139	26.1	1.51	2.811	12.8	90
8	154	26.2	1.51	2.811	12.8	90
8	168	26.3	1.51	2.820	13.2	90
8	181	26.1	1.50	2.837	13.8	88
8	195	26.4	1.51	2.821	13.2	90
8	217	26.7	1.49	2.848	14.3	89
8	237	26.9	1.51	2.816	13.0	92
8	247	27.0	1.51	2.820	13.2	92
8	273	27.0	1.50	2.830	13.5	91
8	286	27.5	1.51	2.820	13.2	94
8	307	27.5	1.51	2.823	13.3	94

Table A- 6. Final water content (w) and dry density (ρ_d) along the samples of GAP-vapour tests under 6 MPa (distance from sample bottom)

Sample	Distance (cm)	*w* (%)	ρ_d (g/cm^3)	Distance (cm)	*w* (%)	ρ_d (g/cm^3)	Distance (cm)	*w* (%)	ρ_d (g/cm^3)
1	2.34	24.7	1.37	1.41	25.1	1.46	0.47	24.5	1.48
2	2.36	25.4	1.40	1.42	25.1	1.45	0.47	24.6	1.51
3	2.26	22.4	1.29	1.35	22.1	1.54	0.45	22.6	1.46
4	2.30	23.0	1.35	1.38	23.0	1.50	0.46	21.9	1.53
9	2.26	22.2	1.42	1.36	21.5	1.53	0.45	20.9	1.55
10	2.26	22.7	1.40	1.35	21.8	1.50	0.45	21.1	1.53
6	2.34	24.9	1.43	1.41	24.8	1.50	0.47	25.2	1.53
7	2.35	25.6	1.40	1.41	25.1	1.50	0.47	25.5	1.53
11	2.25	22.4	1.44	1.35	23.0	1.50	0.45	22.4	1.53
12	2.27	22.9	1.46	1.36	22.1	1.50	0.45	21.8	1.53
5	2.42	26.0	1.43	1.45	23.4	1.44	0.48	24.0	1.50
8	2.35	25.7	1.44	1.41	24.4	1.47	0.47	24.4	1.54

Table A- 7.Pore size distribution obtained with MIP of samples from of GAP-vapour tests under 6 MPa (distance from sample bottom; e: void ratio; M: pores >200 nm; m: pores <200 nm)

Ref.	ρ_d (g/cm^3)	*w* (%)	Distance (cm)	Time (days)	Mode M (nm)	Mode m (nm)	e intruded (%)	non-intruded *e*	e_M	e_m	e_m/e_M
Initial	1.69	13.5	-	-	18,807	11	64	0.215	0.199	0.398	2.00
9.1	1.42	22.2	2.26	14	53,600	17	54	0.414	0.531	0.371	0.70
9.2	1.53	21.5	1.36	14	16,933	11	60	0.309	0.273	0.492	1.81
9.3	1.55	20.9	0.45	14	13,710	12	59	0.308	0.247	0.495	2.00
10.1	1.40	22.7	2.26	14	31,696	8	48	0.481	0.568	0.361	0.64
10.2	1.50	21.8	1.35	14	250,308	11	56	0.349	0.266	0.534	2.01
10.3	1.53	21.1	0.45	14	59,486	15	51	0.376	0.198	0.567	2.86
3.1	1.29	22.4	2.26	29	66,042	9	49	0.556	0.730	0.363	0.50
3.2	1.54	22.1	1.35	29	35,216	11	58	0.314	0.259	0.494	1.91
3.3	1.46	22.6	0.45	29	43,404	21	53	0.399	0.271	0.579	2.14
4.1	1.36	23.0	2.30	29	18,796	19	50	0.496	0.632	0.353	0.56
4.2	1.50	23.0	1.38	29	35,230	10	56	0.354	0.267	0.533	2.00
4.3	1.53	21.9	0.46	29	48,219	12	60	0.306	0.270	0.495	1.83
11.1	1.44	22.4	2.25	32	20,892	12	57	0.379	0.544	0.331	0.61
11.2	1.50	23.0	1.35	32	48,269	12	56	0.35	0.267	0.533	1.99
11.3	1.53	22.4	0.45	32	66,092	12	58	0.322	0.260	0.504	1.94
12.1	1.46	22.9	2.27	32	39,110	10	56	0.377	0.495	0.354	0.71
12.2	1.50	22.1	1.36	32	43,417	11	56	0.349	0.269	0.531	1.97
12.3	1.53	21.8	0.45	32	462,653	7	56	0.338	0.232	0.533	2.29
1.1	1.37	24.7	2.34	64	48,230	12	53	0.455	0.355	0.615	1.73
1.2	1.46	25.1	1.41	64	81,178	10	52	0.407	0.287	0.562	1.96
1.3	1.48	24.5	0.47	64	99,558	15	72	0.228	0.420	0.404	0.96
2.1	1.40	25.4	2.36	64	43,413	7	52	0.443	0.314	0.614	1.95
2.2	1.45	25.1	1.42	64	66,115	8	52	0.412	0.289	0.573	1.99
2.3	1.51	24.6	0.47	64	462,959	12	74	0.205	0.433	0.355	0.82
6.1	1.43	24.9	2.34	106	48,269	11	54	0.409	0.298	0.590	1.98
6.2	1.50	24.8	1.41	106	53,585	14	59	0.329	0.288	0.512	1.78
6.3	1.53	25.2	0.47	106	122,165	12	60	0.304	0.270	0.495	1.83
7.1	1.40	25.6	2.35	106	73,207	10	57	0.402	0.338	0.591	1.75
7.2	1.50	25.1	1.41	106	35,235	12	55	0.356	0.272	0.528	1.94
7.3	1.53	25.5	0.47	106	99,580	11	58	0.318	0.271	0.493	1.82
5.1	1.43	26.0	2.42	307	35,217	15	49	0.455	0.254	0.635	2.50
5.2	1.44	23.4	1.45	307	43,380	11	51	0.425	0.269	0.606	2.26
5.3	1.50	24.0	0.48	307	48,216	14	53	0.379	0.245	0.555	2.26
8.1	1.44	25.7	2.35	307	89,907	9	63	0.325	0.373	0.502	1.35
8.2	1.44	24.4	1.41	307	43,380	11	51	0.425	0.270	0.605	2.24
8.3	1.54	24.4	0.47	307	48,209	11	56	0.330	0.233	0.521	2.24

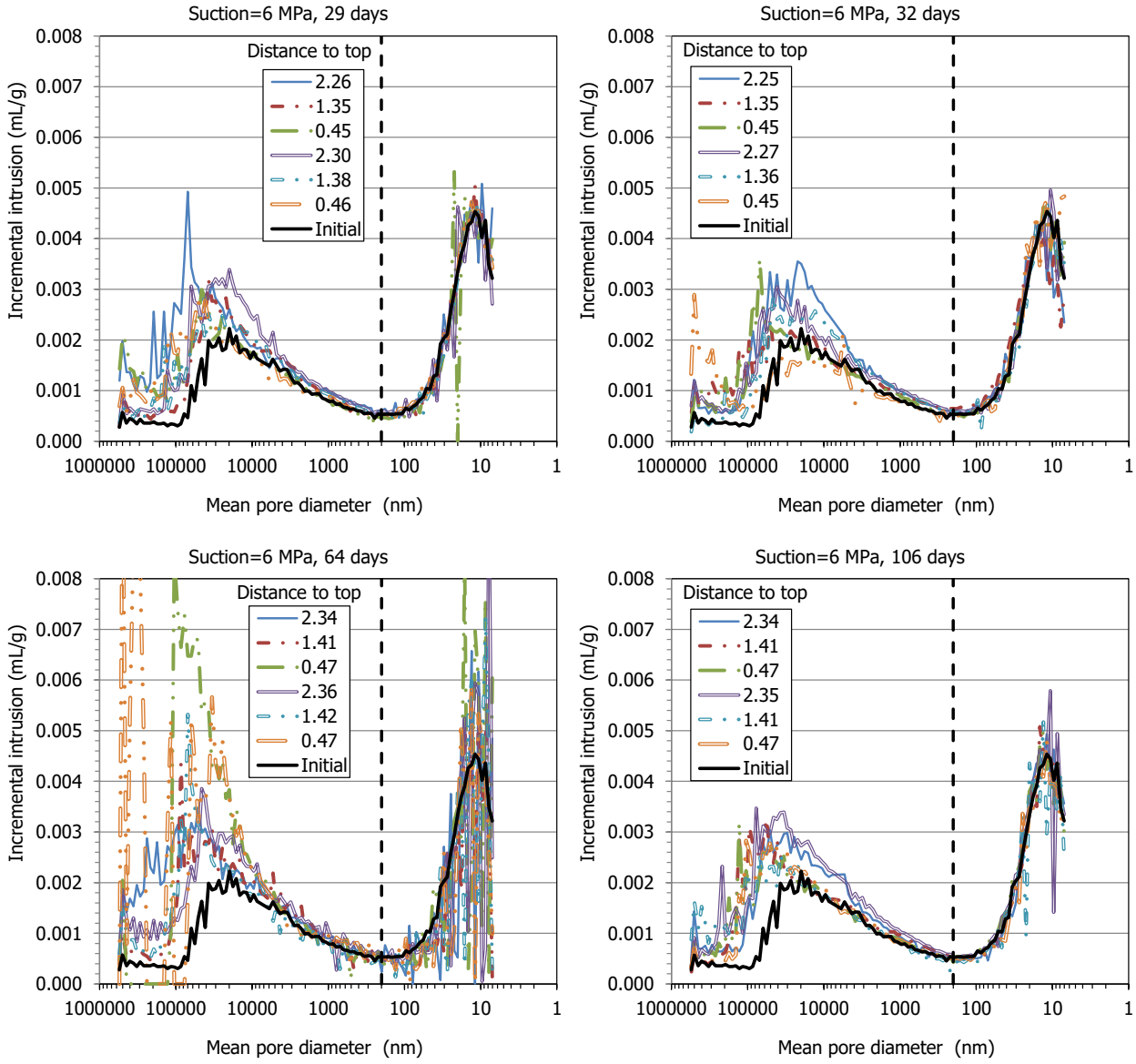

Figure A- 1: Pore size distribution of subsamples tested in GAP-vapour cells under suction 6 MPa for different times and for the initial block expressed as incremental mercury intrusion (duplicate samples for each duration, distances in cm)

GAP VAPOUR TEST RESULTS UNDER SUCTION 0.5 MPa

Table A- 8. Results of duplicate tests (initial ρ_d=1.7 g/cm^3, initial w=14%, initial h=2.5 cm) under s=0.5 MPa of duration 14 days

Sample	Time (days)	*w* (%)	ρ_d (g/cm^3)	h (cm)	$\Delta h/h_o$ (%)	S_r (%)
19	0	13.1	1.69	2.515	0	59
19	6	16.4	1.65	2.575	2.39	70
19	14	18.3	1.63	2.615	4	75
20	0	13.1	1.68	2.531	0	58
20	6	16.3	1.64	2.591	2.37	68
20	14	18	1.62	2.630	3.9	73

Table A- 9. Results of tests (initial ρ_d=1.7 g/cm^3, initial w=14%, initial h=2.5 cm) under s=0.5 MPa of duration 1 month

Sample	Time (days)	*w* (%)	ρ_d (g/cm^3)	h (cm)	$\Delta h/h_o$ (%)	S_r (%)
21	0	14.4	1.70	2.498	0.0	66
21	13	19.4	1.62	2.630	5.3	78
21	20	20.9	1.60	2.653	6.2	82
21	29	21.7	1.57	2.701	8.1	82
22	0	14.4	1.70	2.502	0.0	66
22	13	18.9	1.62	2.617	4.6	77
22	20	20.5	1.61	2.641	5.6	82
22	29	21.5	1.59	2.671	6.8	83
17	0	13.1	1.69	2.510	0.0	59
17	14	18.5	1.65	2.573	2.5	79
17	20	18.3	1.63	2.610	4.0	75
17	27	19.6	1.60	2.651	5.6	77
18	0	13.1	1.71	2.485	0.0	61
18	14	16.9	1.65	2.569	3.4	72
18	20	18.1	1.63	2.610	5.1	74
18	27	19.8	1.62	2.630	5.8	80

Table A- 10. Results of duplicate tests (initial ρ_d=1.7 g/cm^3, initial w=14%, initial h=2.5 cm) under s=0.5 MPa of duration 3 months

Sample	Time (days)	*w* (%)	ρ_d (g/cm^3)	h (cm)	$\Delta h/h_o$ (%)	S_r (%)
15	0	13.1	1.71	2.479	0.0	61
15	13	22.3	1.60	2.662	7.4	87
15	29	25.0	1.56	2.728	10.0	92
15	42	25.6	1.55	2.744	10.7	93
15	55	26.7	1.54	2.761	11.4	96
15	69	27.7	1.54	2.764	11.5	99
15	84	28.9	1.52	2.791	12.6	101
15	97	29.3	1.51	2.809	13.3	101
16	0	13.1	1.70	2.499	0.0	60
16	13	23.4	1.57	2.712	8.5	87
16	29	25.8	1.55	2.743	9.7	94
16	42	26.4	1.52	2.806	12.3	91
16	55	27.8	1.53	2.774	11.0	98
16	69	29.5	1.52	2.806	12.3	102
16	84	30.2	1.49	2.856	14.3	100
16	97	30.1	1.52	2.790	11.6	105

Table A- 11. Results of duplicate tests (initial ρ_d=1.7 g/cm^3, initial w=14%, initial h=2.5 cm) under s=0.5 MPa of duration 6 months

Sample	Time (days)	*w* (%)	ρ_d (g/cm^3)	h (cm)	$\Delta h/h_o$ (%)	S_r (%)
23	0	14.4	1.69	2.514	0.0	65
23	14	24.8	1.47	2.890	14.9	80
23	33	28.2	1.45	2.932	16.6	88
23	47	29.7	1.45	2.923	16.3	93
23	62	30.8	1.45	2.934	16.7	96
23	88	32.0	1.45	2.937	16.8	100
23	106	32.4	1.45	2.936	16.8	101
23	124	32.5	1.45	2.936	16.8	101
23	138	33.2	1.44	2.941	17.0	103
23	159	33.8	1.44	2.949	17.3	104
23	180	33.8	1.44	2.947	17.2	104
24	0	14.4	1.70	2.492	0.0	66
24	14	24.7	1.47	2.894	16.1	80
24	33	28.3	1.45	2.923	17.3	89
24	47	29.6	1.45	2.932	17.7	92
24	62	30.6	1.45	2.937	17.9	95
24	88	32.2	1.44	2.953	18.5	99
24	106	32.6	1.43	2.965	19.0	100
24	124	33.2	1.44	2.958	18.7	102
24	138	33.5	1.44	2.958	18.7	103
24	159	33.6	1.43	2.966	19.0	102
24	180	33.7	1.43	2.964	19.0	103

Table A- 12. Results of duplicate tests (initial ρ_d=1.7 g/cm^3, initial w=14%, initial h=2.5 cm) under s=0.5 MPa of duration 8 months

Sample	Time (days)	*w* (%)	ρ_d (g/cm^3)	h (cm)	$\Delta h/h_o$ (%)	S_r (%)
13	0	13.1	1.72	2.477	0.0	61
13	13	22.2	1.59	2.679	8.1	85
13	29	24.7	1.56	2.733	10.3	91
13	42	25.5	1.54	2.757	11.3	92
13	55	26.5	1.53	2.775	12.0	94
13	69	27.2	1.52	2.788	12.5	95
13	84	28.5	1.51	2.811	13.5	98
13	111	29.5	-	-	-	-
13	132	30.5	-	-	-	-
13	146	30.7	-	-	-	-
13	175	30.5	1.43	2.966	19.8	93
13	189	30.6	1.43	2.968	19.8	93
13	210	30.4	1.44	2.960	19.5	93
13	233	30.5	1.44	2.962	19.6	93
13	246	30.5	1.43	2.968	19.8	93
14	0	13.1	1.72	2.471	0.0	62
14	13	22.9	1.58	2.698	9.2	87
14	29	25.5	1.52	2.792	13.0	89
14	42	26.3	1.52	2.798	13.2	91
14	55	27.6	1.51	2.813	13.9	95
14	69	28.4	1.51	2.821	14.2	97
14	84	29.2	1.49	2.844	15.1	98
14	111	29.8	-	-	-	-
14	132	31.0	-	-	-	-
14	146	31.1	-	-	-	-
14	175	31.4	1.43	2.782	20.7	95
14	189	31.4	1.43	2.966	20.0	96
14	210	31.1	1.44	2.955	19.6	96
14	233	31.1	1.44	2.944	19.2	97
14	246	31.1	1.44	2.952	19.5	96

Table A- 13. Results of duplicate tests (initial ρ_d=1.7 g/cm^3, initial w=14%, initial h=2.5 cm) under s=0.5 MPa of duration 15.5 months

Sample	Time (days)	*w* (%)	ρ_d (g/cm^3)	h (cm)	$\Delta h/h_o$ (%)	S_r (%)
25	0	14.4	1.71	2.491	0.0	67
25	14	24.5	1.51	2.819	13.2	84
25	33	27.7	1.44	2.946	18.3	86
25	47	29.0	1.45	2.925	17.4	91
25	62	29.8	1.46	2.913	16.9	95
25	88	31.9	1.44	2.950	18.4	99
25	106	33.1	1.44	2.946	18.3	102
25	124	33.5	1.44	2.948	18.3	104
25	138	33.7	1.44	2.953	18.6	104
25	159	34.0	1.44	2.951	18.5	105
25	180	34.2	1.43	2.962	18.9	105
25	197	34.3	1.43	2.963	19.0	105
25	209	34.4	1.43	2.967	19.1	105
25	225	34.6	1.43	2.973	19.3	105
25	243	34.0	1.44	2.957	18.7	104
25	260	33.5	1.44	2.952	18.5	103
25	292	33.6	1.45	2.936	17.9	105
25	312	33.6	1.45	2.939	18.0	105
25	323	33.7	1.44	2.951	18.5	104
25	350	33.8	1.44	2.944	18.2	105
25	412	34.1	1.44	2.955	18.6	105
25	447	34.3	1.44	2.955	18.6	106
25	466	34.1	1.44	2.954	18.6	105
26	0	14.4	1.71	2.487	0.0	67
26	14	25.2	1.50	2.827	13.7	85
26	33	28.3	1.44	2.960	19.0	87
26	47	30.1	1.44	2.943	18.3	93
26	62	31.0	1.45	2.937	18.1	97
26	88	32.6	1.44	2.955	18.8	100
26	106	33.3	1.44	2.958	18.9	102
26	124	33.2	1.44	2.956	18.9	102
26	138	33.8	1.44	2.961	19.1	104
26	159	34.6	1.43	2.968	19.4	105
26	180	34.7	1.43	2.969	19.4	106
26	197	34.6	1.43	2.964	19.2	106
26	209	34.7	1.44	2.962	19.1	106
26	225	34.6	1.43	2.966	19.3	106
26	243	34.4	1.43	2.964	19.2	105
26	260	34.0	1.44	2.961	19.0	104
26	292	33.7	1.44	2.950	18.6	104
26	312	32.9	1.45	2.935	18.0	103
26	323	32.6	1.45	2.929	17.8	102
26	350	32.0	1.45	2.923	17.5	101
26	412	34.2	1.44	2.955	18.8	105
26	447	34.5	1.44	2.957	18.8	106
26	466	34.3	1.44	2.957	18.9	106

Table A- 14. Final water content (w) and dry density (ρ_d) along the samples of GAP-vapour tests under 0.5 MPa (distance from sample bottom)

Sample	Distance (cm)	*w (%)*	ρ_d (g/cm^3)	Distance (cm)	*w (%)*	ρ_d (g/cm^3)	Distance (cm)	*w* (%)	ρ_d (g/cm^3)
17	2.21	19.9	-	1.33	19.2	1.54	0.44	19.5	1.58
18	2.19	19.4	1.50	1.31	19.2	-	0.44	19.2	-
19	2.18	18.0	-	1.31	17.4	1.59	0.44	17	1.59
20	2.19	16.8	1.54	1.31	16.8	1.60	0.44	17.1	-
15	2.34	28.7	1.42	1.40	28.0	1.46	0.47	27.1	1.49
16	2.32	30.0	1.35	1.39	29.6	1.41	0.46	29.4	1.47
21	2.25	20.6	1.53	1.35	20.6	1.57	0.45	20	1.56
22	2.23	19.7	-	1.34	19.8	1.56	0.45	19.6	1.57
13	2.47	33.0	1.36	1.48	32.1	1.42	0.49	31.6	1.42
14	2.46	33.6	1.36	1.48	32.2	1.40	0.49	32.6	1.54
23	2.46	34.0	1.39	1.47	32.3	1.42	0.49	32.3	1.41
24	2.47	33.1	1.38	1.48	32.9	1.41	0.49	32.5	1.42
25	2.46	32.8	1.40	1.48	32.4	1.43	0.49	32.5	1.46
26	2.46	33.6	1.40	1.48	32.1	1.40	0.49	32.5	1.43

Table A- 15. Pore size distribution obtained with MIP of samples from of GAP-vapour tests under 0.5 MPa (distance from sample bottom; e: void ratio; M: pores >200 nm; m: pores <200 nm)

Sample	ρ_d (g/cm^3)	*w* (%)	Distance (cm)	Time (days)	Mode M (nm)	Mode m (nm)	e intruded (%)	non-intruded *e*	e_M	e_m	e_m/e_M
Initial	1.69	13.5	-	-	18,807	11	64	0.215	0.199	0.398	2.00
19.1	1.58	18.0	2.18	14	20,882	10	62	0.272	0.345	0.364	1.05
19.2	1.59	17.4	1.31	14	459,429	11	59	0.288	0.223	0.475	2.13
19.3	1.59	17.0	0.44	14	28,550	17	51	0.343	0.200	0.498	2.48
20.1	1.54	16.8	2.19	14	9,023	9	54	0.344	0.390	0.363	0.93
20.2	1.60	16.8	1.31	14	31,697	12	57	0.294	0.219	0.468	2.13
20.3	1.65	17.1	0.44	14	53,545	9	64	0.226	0.237	0.399	1.68
17.1	1.51	19.9	2.21	27	456,813	17	61	0.308	0.441	0.347	0.79
17.2	1.54	19.2	1.33	27	20,892	10	59	0.308	0.261	0.492	1.88
17.3	1.58	19.5	0.44	27	18,796	7	57	0.307	0.207	0.501	2.42
18.1	1.50	19.4	2.19	27	31,719	14	59	0.325	0.459	0.341	0.74
18.2	1.54	19.2	1.31	27	20,893	11	55	0.339	0.231	0.522	2.26
18.3	1.58	19.2	0.44	27	6,279	14	54	0.326	0.193	0.516	2.67
21.1	1.53	20.6	2.25	29	16,934	7	60	0.306	0.404	0.360	0.89
21.2	1.57	20.6	1.35	29	13,713	12	57	0.313	0.221	0.499	2.26
21.3	1.56	20.0	0.45	29	66,059	7	61	0.282	0.255	0.476	1.87
22.1	1.53	19.7	2.23	29	461,924	15	58	0.318	0.402	0.363	0.90
22.2	1.56	19.8	1.34	29	35,233	14	58	0.309	0.228	0.503	2.21
22.3	1.57	19.6	0.45	29	18,802	14	62	0.276	0.258	0.462	1.79
15.1	1.42	28.7	2.34	97	43,411	10	53	0.420	0.312	0.590	1.89
15.2	1.46	28.0	1.40	97	59,463	10	46	0.455	0.227	0.622	2.73
15.3	1.47	27.1	0.47	97	81,153	11	44	0.466	0.203	0.634	3.13
16.1	1.35	30.0	2.32	97	81,079	15	52	0.479	0.352	0.648	1.84
16.2	1.41	29.6	1.39	97	48,231	8	50	0.461	0.279	0.635	2.27
16.3	1.47	29.4	0.46	97	66,049	9	42	0.482	0.183	0.654	3.57
13.1	1.36	33.0	2.47	246	39,107	9	61	0.382	0.429	0.556	1.29
13.2	1.42	32.1	1.48	246	20,881	10	60	0.364	0.354	0.547	1.55
13.3	1.42	31.6	0.49	246	48,234	10	56	0.400	0.321	0.581	1.81
14.1	1.36	33.6	2.46	246	48,258	29	63	0.366	0.445	0.541	1.22
14.2	1.40	32.2	1.48	246	53,594	9	59	0.376	0.373	0.556	1.49
14.3	1.54	32.6	0.49	246	31,700	10	68	0.239	0.334	0.419	1.26
23.1	1.39	34.0	2.46	180	25,728	12	61	0.371	0.394	0.548	1.39
23.2	1.42	32.3	1.47	180	18,793	10	64	0.329	0.397	0.504	1.27
23.3	1.41	32.3	0.49	180	28,546	8	60	0.369	0.363	0.552	1.52
24.1	1.38	33.1	2.47	180	23,168	11	57	0.408	0.389	0.568	1.46
24.2	1.41	32.9	1.48	180	28,542	12	65	0.323	0.419	0.496	1.18
24.3	1.42	32.5	0.49	180	18,794	14	60	0.361	0.363	0.539	1.49
25.1	1.40	32.8	2.46	466	35,235	15	60	0.373	0.371	0.557	1.50
25.2	1.43	32.4	1.48	466	39,116	12	64	0.321	0.386	0.503	1.30
25.3	1.46	32.5	0.49	466	23,182	12	61	0.331	0.349	0.500	1.43
26.1	1.40	33.6	2.46	466	25,730	9	63	0.341	0.402	0.527	1.31
26.2	1.40	32.1	1.48	466	35,226	14	62	0.356	0.384	0.544	1.42
26.3	1.43	32.5	0.49	466	43,434	12	56	0.389	0.303	0.586	1.93

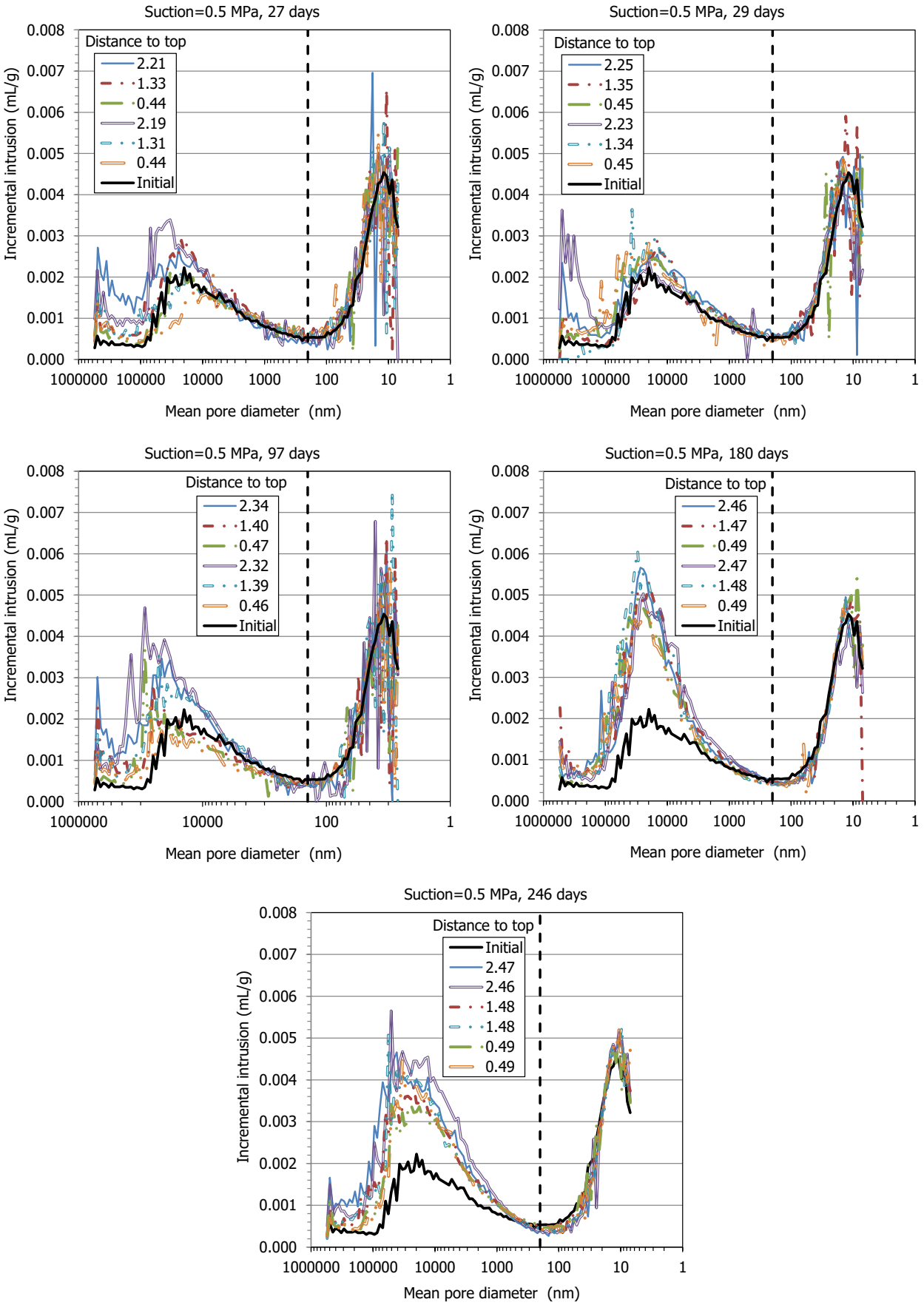

Figure A- 2. Pore size distribution of subsamples tested in GAP-vapour cells under suction 0.5 MPa for different times and for the initial block expressed as incremental mercury intrusion (duplicate samples for each duration, distances in cm)

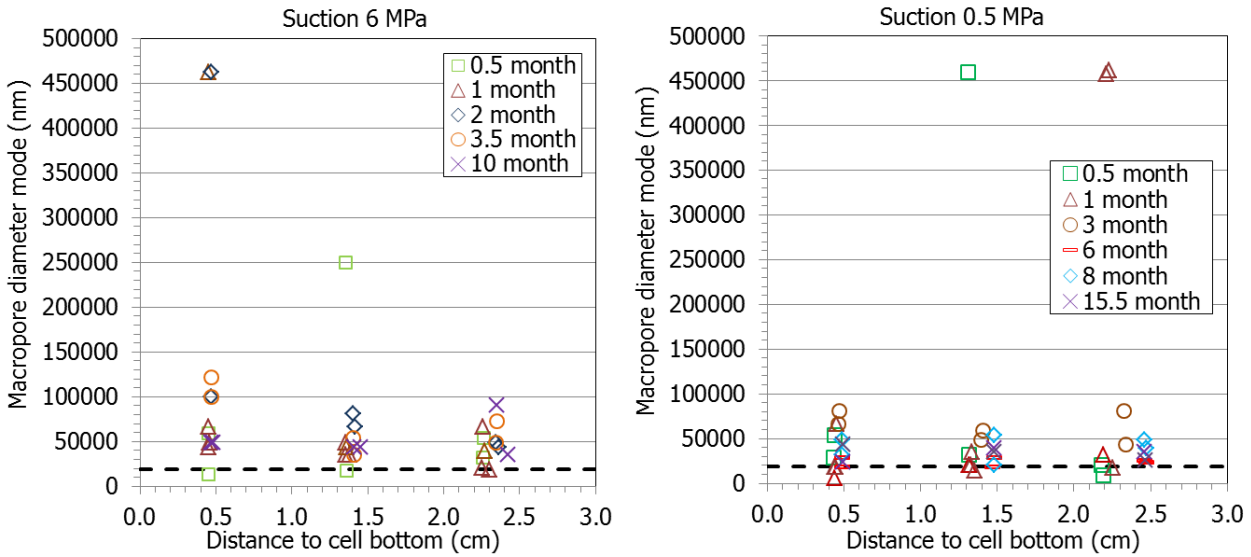

Figure A- 3. Mode size of macropores of subsamples tested in GAP-vapour cells under suction 6 MPa (left) and 0.5 MPa (right) for different times and as a function of the position of the subsample (hydration from top; duplicate samples for each duration)

GAP LIQUID TESTS ONLINE RESULTS

Table A- 16. Online results test GL1, duration 66 days (injection opposite to gap, initial ρ_d=1.65 g/cm^3, initial w=13.3%)

Injection pressure (MPa)	Time[a] (h)	Water intake[a] (cm^3)	Time[b] (h)	Water intake[b] (cm^3)	Injection pressure (MPa)	Time[a] (h)	Water intake[a] (cm^3)	Time[b] (h)	Water intake[b] (cm^3)
0.006	0	0.000	-	-	0.345	476	34.688	364	26.188
0.006	12	1.361	-	-	0.386	500	36.417	388	26.620
0.006	24	2.193	-	-	0.408	524	38.146	412	26.620
0.007	36	3.058	-	-	0.472	548	39.876	436	26.620
0.007	48	3.922	-	-	0.492	569	41.441	458	26.620
0.007	60	4.787	-	-	0.539	593	43.170	482	26.620
0.007	72	5.651	-	-	0.589	617	44.899	506	26.620
0.006	84	6.516	-	-	0.646	641	46.628	530	26.620
0.005	96	7.381	-	-	0.71	665	48.358	554	26.620
0.006	108	8.245	-	-	0.807	689	50.087	578	26.620
0.006	112	8.533	0	0.033	0.915	713	51.816	602	26.620
0.006	114	8.678	2	0.178	1.014	737	53.195	626	26.620
0.006	120	9.110	8	0.610	1.199	761	54.925	650	26.620
0.006	126	9.542	14	1.042	1.339	785	56.654	674	26.620
0.003	132	9.974	20	1.474	1.492	809	58.383	698	26.620
-0.001	138	10.407	26	1.907	1.576	833	60.112	722	26.620
0.000	144	10.839	32	2.339	1.708	857	61.841	746	26.620
0.001	150	11.271	38	2.771	1.857	881	63.571	752	26.620
0.001	156	11.704	44	3.204	1.947	905	64.241	776	26.620
0.003	162	12.136	50	3.636	0.392	929	64.241	800	26.620
0.006	168	12.568	56	4.068	0.143	953	64.241	824	26.620
0.009	174	13.000	62	4.500	0.052	977	64.241	848	26.620
0.01	180	13.433	68	4.933	0.045	1001	64.241	872	26.620
0.013	186	13.865	74	5.365	0.035	1025	64.241	896	26.620
0.017	192	14.298	80	5.798	0.038	1049	65.507	920	26.620
0.021	198	14.730	86	6.230	1.818	1073	66.031	944	26.620
0.024	204	15.162	92	6.662	1.435	1097	66.031	968	26.620
0.028	210	15.594	98	7.094	1.364	1121	66.031	992	26.620
0.036	216	16.027	104	7.527	1.162	1145	66.031	1016	26.620
0.044	222	16.459	110	7.959	0.788	1169	66.031	1040	26.620
0.049	228	16.891	116	8.391	0.693	1193	66.031	1064	26.620
0.055	234	17.324	122	8.824	0.676	1217	66.031	1088	26.620
0.068	240	17.756	128	9.256	0.73	1241	66.031	1112	26.620
0.085	246	18.188	134	9.688	0.833	1265	66.031	1136	26.620
0.094	252	18.621	140	10.121	0.747	1289	66.031	1160	26.620
0.108	258	19.053	146	10.553	0.817	1313	66.031	1184	26.620
0.208	284	20.926	172	12.426	0.792	1337	66.031	1226	26.620
0.335	308	22.583	196	14.083	0.756	1361	66.031	1250	26.620
0.338	332	24.313	220	15.813	0.711	1385	66.031	1274	26.620
0.263	356	26.042	244	17.542	0.716	1409	66.031	1298	26.620
0.212	380	27.771	268	19.271	0.693	1433	66.031	1322	26.620
0.227	404	29.500	292	21.000	0.662	1457	66.031	1346	26.620
0.256	428	31.230	316	22.730	0.374	1481	66.031	1370	26.620
0.304	452	32.959	340	24.459	0.415	1505	66.031	1394	26.620

[a] from the beginning of the experiment, including cell elements; [b] from the moment the bentonite starts to get water (estimation made considering the actual water intake checked at the end of the test)

Table A- 17. Online results test GL2, duration 14 days (injection opposite to gap, initial ρ_d=1.67 g/cm^3, initial w=13.3%)

Injection pressure (MPa)	Time[a] (h)	Water intake[a] (cm^3)	Time[b] (h)	Water intake[b] (cm^3)	Injection pressure (MPa)	Time[a] (h)	Water intake[a] (cm^3)	Time[b] (h)	Water intake[b] (cm^3)
0.007	0	0.000	-	-	0.036	199	14.358	84	6.188
0.007	12	0.873	-	-	0.039	205	14.790	90	6.620
0.007	24	1.738	-	-	0.043	211	15.222	96	7.052
0.007	37	2.685	-	-	0.043	217	15.655	102	7.485
0.007	49	3.550	-	-	0.044	223	16.087	108	7.917
0.007	61	4.415	-	-	0.042	229	16.519	114	8.349
0.007	73	5.279	-	-	0.042	235	16.952	120	8.782
0.007	85	6.144	-	-	0.045	241	17.384	126	9.214
0.007	97	7.008	-	-	0.054	247	17.816	132	9.646
0.007	109	7.873	-	-	0.062	253	18.249	138	10.079
0.007	115	8.306	0	0.136	0.072	259	18.681	144	10.511
0.007	121	8.738	6	0.568	0.085	265	19.113	150	10.943
0.008	127	9.170	12	1.000	0.102	271	19.546	156	11.376
0.008	133	9.602	18	1.432	0.118	277	19.978	162	11.808
0.009	139	10.035	24	1.865	0.134	283	20.410	168	12.240
0.011	145	10.467	30	2.297	0.154	289	20.842	174	12.672
0.013	151	10.899	36	2.729	0.185	295	21.275	180	13.105
0.014	157	11.332	42	3.162	0.208	301	21.707	186	13.537
0.016	163	11.764	48	3.594	0.23	307	22.139	192	13.969
0.018	169	12.196	54	4.026	0.249	313	22.572	198	14.402
0.021	175	12.629	60	4.459	0.275	319	23.004	204	14.834
0.024	181	13.061	66	4.891	0.278	325	23.436	210	15.266
0.027	187	13.493	72	5.323	0.274	331	23.868	216	15.698
0.031	193	13.925	78	5.755	0.269	336	24.224	221	16.054

[a] from the beginning of the experiment, including cell elements; [b] from the moment the bentonite starts to get water (estimation made considering the actual water intake checked at the end of the test)

Table A- 18. Online results test GL3, duration 28 days (injection opposite to gap, initial ρ_d=1.67 g/cm^3, initial w=13.8%)

Injection pressure (MPa)	Time[a] (h)	Water intake[a] (cm^3)	Time[b] (h)	Water intake[b] (cm^3)	Injection pressure (MPa)	Time[a] (h)	Water intake[a] (cm^3)	Time[b] (h)	Water intake[b] (cm^3)
0.007	0	0.000	-	-	0.032	205	14.789	84	6.319
0.007	12	0.864	-	-	0.047	229	16.518	108	8.048
0.007	24	1.729	-	-	0.081	253	18.248	132	9.778
0.007	37	2.685	-	-	0.142	277	19.977	156	11.507
0.007	49	3.549	-	-	0.235	301	21.706	180	13.236
0.007	61	4.414	-	-	0.284	325	23.435	204	14.965
0.007	73	5.279	-	-	0.23	349	25.165	228	16.695
0.007	85	6.143	-	-	0.192	373	26.894	252	18.424
0.007	97	7.008	-	-	0.211	397	28.623	276	20.153
0.007	109	7.872	-	-	0.243	421	30.352	300	21.882
0.007	121	8.737	0	0.267	0.274	445	32.081	324	23.611
0.007	127	9.169	6	0.699	0.306	469	33.811	348	25.341
0.007	133	9.601	12	1.131	0.338	493	35.540	372	26.205
0.007	139	10.034	18	1.564	0.366	517	37.269	396	26.205
0.007	145	10.466	24	1.996	0.39	541	38.998	420	26.205
0.008	151	10.899	30	2.429	0.421	565	40.728	444	26.205
0.01	157	11.331	36	2.861	0.455	589	42.457	468	26.205
0.01	163	11.763	42	3.293	0.494	613	44.186	492	26.205
0.012	169	12.196	48	3.726	0.53	637	45.915	516	26.205
0.015	175	12.628	54	4.158	0.592	661	47.644	546	26.205
0.018	181	13.060	60	4.590	0.597	668	48.171	547	26.205

[a] from the beginning of the experiment, including cell elements; [b] from the moment the bentonite starts to get water (estimation made considering the actual water intake checked at the end of the test)

Table A- 19. Online results test GL4, duration 7 days (injection opposite to gap, initial ρ_d=1.67 g/cm^3, initial w=14.3%)

Injection pressure (MPa)	Time[a] (h)	Water intake[a] (cm^3)	Time[b] (h)	Water intake[b] (cm^3)	Injection pressure (MPa)	Time[a] (h)	Water intake[a] (cm^3)	Time[b] (h)	Water intake[b] (cm^3)
0.007	0	0.000	-	-	0.005	112	8.090	32	2.377
0.008	12	0.880	-	-	0.006	116	8.380	36	2.665
0.01	24	1.750	-	-	0.006	120	8.660	40	2.953
0.013	36	2.610	-	-	0.006	124	8.950	44	3.241
0.005	48	3.480	-	-	0.006	128	9.240	48	3.530
0.005	60	4.340	-	-	0.006	132	9.530	52	3.818
0.004	72	5.210	-	-	0.006	136	9.820	56	4.106
0.005	80	5.780	0	0.071	0.006	140	10.100	60	4.394
0.005	84	6.070	4	0.359	0.006	144	10.390	64	4.682
0.004	88	6.360	8	0.648	0.006	148	10.680	68	4.971
0.004	92	6.650	12	0.936	0.007	152	10.970	72	5.259
0.005	96	6.930	16	1.224	0.007	156	11.260	76	5.547
0.005	100	7.220	20	1.512	0.008	160	11.550	80	5.835
0.005	104	7.510	24	1.800	0.009	164	11.830	84	6.123
0.005	108	7.800	28	2.089	0.01	167	12.050	87	6.340

[a] from the beginning of the experiment, including cell elements; [b] from the moment the bentonite starts to get water (estimation made considering the actual water intake checked at the end of the test)

Table A- 20. Online results test GL5, duration 4 days (injection opposite to gap, initial ρ_d=1.66 g/cm^3, initial w=14.4%)

Injection pressure (MPa)	Time[a] (h)	Water intake[a] (cm^3)	Time[b] (h)	Water intake[b] (cm^3)	Injection pressure (MPa)	Time[a] (h)	Water intake[a] (cm^3)	Time[b] (h)	Water intake[b] (cm^3)
0.004	0	0.000	-	-	0.003	67	4.812	24	1.752
0.003	12	0.861	-	-	0.003	71	5.099	28	2.039
0.003	24	1.723	-	-	0.003	75	5.386	32	2.326
0.002	32	2.298	-	-	0.003	79	5.674	36	2.614
0.002	43	3.088	0	0.028	0.003	83	5.961	40	2.901
0.003	47	3.375	4	0.315	0.003	87	6.248	44	3.188
0.003	51	3.663	8	0.603	0.003	91	6.536	48	3.476
0.003	55	3.950	12	0.890	0.003	95	6.823	52	3.763
0.003	59	4.237	16	1.177	0.003	96	6.895	53	3.835
0.003	63	4.524	20	1.464	-	-	-	-	-

[a] from the beginning of the experiment, including cell elements; [b] from the moment the bentonite starts to get water (estimation made considering the actual water intake checked at the end of the test)

Table A- 21. Online results test GL12, duration 10 days (injection from gap, initial ρ_d=1.69 g/cm^3, initial w=13.1%)

Injection pressure (MPa)	Time[a] (h)	Water intake[a] (cm^3)	Time[b] (h)	Water intake[b] (cm^3)	Injection pressure (MPa)	Time[a] (h)	Water intake[a] (cm^3)	Time[b] (h)	Water intake[b] (cm^3)
-0.004	0	0.000	-	-	0.007	157	11.315	52	3.780
-0.004	12	0.868	-	-	0.009	161	11.603	56	4.060
-0.005	24	1.732	-	-	0.01	165	11.891	60	4.350
-0.004	36	2.597	-	-	0.012	169	12.180	64	4.640
-0.004	48	3.461	-	-	0.014	173	12.468	68	4.930
-0.004	60	4.326	-	-	0.016	177	12.756	72	5.220
-0.005	72	5.191	-	-	0.018	181	13.044	76	5.500
-0.004	84	6.055	-	-	0.02	185	13.332	80	5.790
-0.003	96	6.920	-	-	0.021	189	13.621	84	6.080
-0.002	105	7.568	0	0.030	0.024	193	13.909	88	6.370
-0.002	109	7.857	4	0.320	0.026	197	14.197	92	6.660
-0.002	113	8.145	8	0.600	0.029	201	14.485	96	6.950
-0.001	117	8.433	12	0.890	0.032	205	14.773	100	7.230
-0.001	121	8.721	16	1.180	0.035	209	15.062	104	7.520
-0.001	125	9.009	20	1.470	0.037	213	15.350	108	7.810
0.0000	129	9.298	24	1.760	0.041	217	15.638	112	8.100
0.0000	133	9.586	28	2.050	0.045	221	15.926	116	8.390
0.001	137	9.874	32	2.330	0.048	225	16.215	120	8.680
0.002	141	10.162	36	2.620	0.053	229	16.503	124	8.960
0.003	145	10.450	40	2.910	0.057	233	16.791	128	9.250
0.004	149	10.739	44	3.200	0.061	237	17.100	132	9.560
0.006	153	11.027	48	3.490					

[a] from the beginning of the experiment, including cell elements; [b] from the moment the bentonite starts to get water (estimation made considering the actual water intake checked at the end of the test)

Table A- 22. Online results test GL6, duration 7 days (injection from gap, initial ρ_d=1.66 g/cm^3, initial w=14.3%)

Injection pressure (MPa)	Time[a] (h)	Water intake[a] (cm^3)	Time[b] (h)	Water intake[b] (cm^3)	Injection pressure (MPa)	Time[a] (h)	Water intake[a] (cm^3)	Time[b] (h)	Water intake[b] (cm^3)
0	0	0.000	-	-	0.012	80	5.798	72	5.210
0.001	8	0.610	0	0.020	0.012	84	6.086	76	5.500
0.001	12	0.898	4	0.310	0.012	88	6.374	80	5.780
0.001	16	1.186	8	0.600	0.013	92	6.662	84	6.070
0.001	20	1.475	12	0.880	0.013	96	6.951	88	6.360
0.002	24	1.763	16	1.170	0.015	100	7.239	92	6.650
0.003	28	2.051	20	1.460	0.016	104	7.527	96	6.940
0.004	32	2.339	24	1.750	0.017	108	7.815	100	7.230
0.004	36	2.628	28	2.040	0.017	112	8.103	104	7.510
0.005	40	2.916	32	2.330	0.017	116	8.392	108	7.800
0.006	44	3.204	36	2.610	0.024	141	10.153	132	9.560
0.006	48	3.492	40	2.900	0.026	145	10.441	136	9.850
0.007	52	3.780	44	3.190	0.027	149	10.729	140	10.140
0.009	56	4.069	48	3.480	0.028	153	11.017	144	10.430
0.009	60	4.357	52	3.770	0.029	157	11.305	148	10.720
0.01	64	4.645	56	4.060	0.029	161	11.594	152	11.000
0.01	68	4.933	60	4.340	0.029	165	11.882	156	11.290
0.01	72	5.221	64	4.630	0.032	167	12.025	158	11.440
0.011	76	5.510	68	4.920	-	-	-	-	-

[a] from the beginning of the experiment, including cell elements; [b] from the moment the bentonite starts to get water (estimation made considering the actual water intake checked at the end of the test)

Table A- 23. Online results test GL7, duration 7 days (injection from gap, initial ρ_d=1.67 g/cm^3, initial w=14.4%)

Injection pressure (MPa)	Time (h)	Water intake (cm^3)	Injection pressure (MPa)	Time (h)	Water intake (cm^3)
0.001	0	2.61[a]	-0.002	88	8.950
0.000	4	2.898	-0.001	92	9.238
0.001	8	3.186	-0.002	96	9.526
0.000	12	3.474	-0.001	100	9.815
0.000	16	3.762	-0.001	104	10.103
0.000	20	4.050	-0.001	108	10.391
0.000	24	4.339	-0.001	112	10.679
0.000	28	4.627	-0.001	116	10.967
0.000	32	4.915	-0.001	120	11.256
0.000	36	5.203	-0.001	124	11.544
0.000	40	5.491	-0.001	128	11.832
0.000	44	5.780	-0.001	132	12.120
0.000	48	6.068	-0.001	136	12.408
0.000	52	6.356	0.000	140	12.697
0.000	56	6.644	-0.001	144	12.985
0.000	60	6.933	0.000	148	13.273
-0.001	64	7.221	0.000	152	13.561
-0.001	68	7.509	-0.001	156	13.849
-0.001	72	7.797	0.000	160	14.138
-0.001	76	8.085	0.000	164	14.426
-0.001	80	8.373	-0.001	166	14.570
-0.001	84	8.662	-	-	-

[a] at the beginning of the test the bentonite had already taken some water from the wet porous stone

Table A- 24. Online results test GL8, duration 22 days (injection from gap, initial ρ_d=1.67 g/cm^3, initial w=14.1%)

Injection pressure (MPa)	Time[a] (h)	Water intake[a] (cm^3)	Time[b] (h)	Water intake[b] (cm^3)	Injection pressure (MPa)	Time[a] (h)	Water intake[a] (cm^3)	Time[b] (h)	Water intake[b] (cm^3)
-0.001	0	0.000	-	-	0.001	177	12.752	114	8.242
0.000	12	0.863	-	-	0.001	183	13.184	120	8.674
0.000	24	1.728	-	-	0.001	189	13.616	126	9.106
0.000	36	2.592	-	-	0.001	195	14.049	132	9.539
0.000	48	3.457	-	-	0.001	201	14.481	138	9.971
0.000	60	4.322	-	-	0.000	207	14.913	144	10.403
0.000	63	4.538	0	0.028	0.000	213	15.346	150	10.836
0.000	69	4.970	6	0.460	0.001	219	15.778	156	11.268
0.000	75	5.403	12	0.893	0.001	225	16.210	162	11.700
0.001	81	5.835	18	1.325	0.001	231	16.642	168	12.132
0.001	87	6.267	24	1.757	0.001	237	17.075	174	12.565
0.000	93	6.699	30	2.189	0.001	243	17.507	180	12.997
0.000	99	7.132	36	2.622	0.001	267	19.236	204	14.726
0.000	105	7.564	42	3.054	0.008	291	20.966	228	16.456
0.000	111	7.996	48	3.486	0.020	315	22.695	252	18.185
-0.001	117	8.429	54	3.919	0.039	339	24.424	276	19.914
-0.001	123	8.861	60	4.351	0.069	363	26.153	300	21.643
0.000	129	9.293	66	4.783	0.117	387	27.883	324	23.373
0.000	135	9.726	72	5.216	0.191	411	29.612	348	25.102
0.000	141	10.158	78	5.648	0.287	435	31.341	372	25.966
0.000	147	10.590	84	6.080	0.405	459	33.070	396	25.966
0.000	153	11.023	90	6.513	0.541	483	34.799	420	25.966
0.000	159	11.455	96	6.945	0.632	507	36.529	444	25.966
0.000	165	11.887	102	7.377	0.703	527	37.970	464	25.966
0.001	171	12.319	108	7.809	-	-	-	-	-

[a] from the beginning of the experiment, including cell elements; [b] from the moment the bentonite starts to get water (estimation made considering the actual water intake checked at the end of the test)

Table A- 25. Online results test GL9, duration 14 days (injection from gap, initial ρ_d=1.70 g/cm^3, initial w=13.6%)

Injection pressure (MPa)	Time (h)	Water intake (cm^3)	Injection pressure (MPa)	Time (h)	Water intake (cm^3)
0.000	0	0.89[a]	-0.002	114	9.101
0.000	6	1.320	-0.003	120	9.533
-0.001	12	1.752	-0.001	126	9.966
-0.001	18	2.184	-0.001	132	10.398
-0.001	24	2.617	-0.001	138	10.830
0.000	30	3.049	0.000	144	11.263
0.000	36	3.481	-0.001	150	11.695
0.000	42	3.913	0.000	156	12.127
0.000	48	4.346	0.000	162	12.560
0.000	54	4.778	0.000	168	12.992
0.000	60	5.210	0.000	174	13.424
0.000	66	5.643	0.000	180	13.856
-0.001	72	6.075	0.000	204	15.586
0.000	78	6.507	0.000	228	17.315
0.000	84	6.940	0.000	252	19.044
-0.001	90	7.372	0.001	276	20.773
-0.001	96	7.804	0.013	300	22.503
0.000	102	8.236	0.030	324	24.232
-0.001	108	8.669	0.041	335	25.062

[a] at the beginning of the test the bentonite had already taken some water from the wet porous stone

Table A- 26. Online results test GL11, duration 2 days (injection from gap, initial ρ_d=1.67 g/cm^3, initial w=14.3%)

Injection pressure (MPa)	Time (h)	Water intake (cm^3)	Injection pressure (MPa)	Time (h)	Water intake (cm^3)
0.000	0	1.94[a]	-0.001	28	3.956
-0.001	4	2.227	-0.001	32	4.244
-0.001	8	2.515	-0.001	36	4.533
-0.001	12	2.803	-0.001	40	4.821
-0.002	16	3.091	-0.001	44	5.109
-0.002	20	3.380	-0.001	48	5.406
-0.001	24	3.668	-	-	-

[a] at the beginning of the test the bentonite had already taken some water from the wet porous stone

Table A- 27. Online results test GL13, duration 39 days (injection from gap, initial ρ_d=1.66 g/cm^3, initial w=14.3%)

Injection pressure (MPa)	Time[a] (h)	Water intake[a] (cm^3)	Time[b] (h)	Water intake[b] (cm^3)	Injection pressure (MPa)	Time[a] (h)	Water intake[a] (cm^3)	Time[b] (h)	Water intake[b] (cm^3)
-0.005	0	0.000	-	-	-0.003	230	16.556	156	11.196
-0.003	12	0.862	-	-	-0.003	236	16.987	162	11.627
-0.003	24	1.724	-	-	-0.003	242	17.418	168	12.058
-0.003	36	2.586	-	-	-0.003	267	19.142	192	13.782
-0.003	48	3.448	-	-	-0.003	291	20.866	216	15.506
-0.003	60	4.310	-	-	0.005	315	22.590	240	17.230
-0.003	72	5.172	-	-	0.02	339	24.313	264	18.953
-0.003	75	5.387	0	0.027	0.039	362	26.037	288	20.677
-0.003	80	5.782	6	0.422	0.067	386	27.761	312	22.401
-0.003	86	6.213	12	0.853	0.111	410	29.485	336	24.125
-0.003	92	6.644	18	1.284	0.167	434	31.209	360	25.849
-0.003	98	7.075	24	1.715	0.242	458	32.932	384	26.136
-0.003	104	7.506	30	2.146	0.313	483	34.656	408	26.136
-0.003	110	7.937	36	2.577	0.38	506	36.380	432	26.136
-0.003	117	8.368	42	3.008	0.371	530	38.104	456	26.136
-0.003	122	8.799	48	3.439	0.49	554	39.828	480	26.136
-0.003	128	9.230	54	3.870	0.306	578	41.552	504	26.136
-0.003	135	9.661	60	4.301	0.673	602	43.275	528	26.136
-0.003	141	10.092	66	4.732	0.658	626	44.999	552	26.136
-0.003	146	10.523	72	5.163	1.165	650	46.723	576	26.136
-0.003	152	10.954	78	5.594	1.034	674	48.447	600	26.136
-0.003	158	11.385	84	6.025	0.989	698	50.171	624	26.136
-0.003	164	11.816	90	6.456	0.928	722	51.894	648	26.136
-0.003	170	12.247	96	6.887	0.896	746	53.618	672	26.136
-0.003	176	12.678	102	7.318	0.856	770	55.342	696	26.136
-0.003	182	13.109	108	7.749	0.818	795	57.066	720	26.136
-0.003	188	13.540	114	8.180	0.789	818	58.790	744	26.136
-0.003	194	13.970	120	8.610	0.78	842	60.442	767	26.136
-0.003	200	14.401	126	9.041	1.075	865	62.166	791	26.136
-0.003	206	14.832	132	9.472	0.949	889	63.889	815	26.136
-0.003	212	15.263	138	9.903	0.879	913	65.613	839	26.136
-0.003	218	15.694	144	10.334	1.148	938	67.409	864	26.136
-0.003	224	16.125	150	10.765					

[a] from the beginning of the experiment, including cell elements; [b] from the moment the bentonite starts to get water (estimation made considering the actual water intake checked at the end of the test)

Table A- 28. Pore size distribution obtained with MIP of samples from of GAP-liquid tests saturated through bottom (distance from sample bottom; e: void ratio; M: pores >200 nm; m: pores <200 nm)

Ref.	ρ_d (g/cm^3)	*w* (%)	Distance (cm)	Time (days)	Mode M (nm)	Mode m (nm)	e intruded (%)	non-intruded *e*	e_M	e_m	e_m/e_M
Initial	1.69	13.5	-	-	18,807	11	64	0.215	0.199	0.398	2.00
GL1.1	1.25	43.3	3.07	63	31,701	11	74	0.306	0.690	0.470	0.68
GL1.2	1.23	43.1	2.20	63	25,724	9	70	0.360	0.689	0.506	0.74
GL1.3	1.22	45.0	1.30	63	23,186	7	72	0.336	0.715	0.499	0.70
GL1.4	1.17	49.4	0.40	63	23,184	7	74	0.334	0.809	0.499	0.62
GL2.1-2	1.36	25.8	2.50	14	278,139	11	66	0.331	0.672	0.313	0.47
GL2.3	1.30	30.1	1.30	14	20,895	11	57	0.467	0.450	0.627	1.39
GL2.4	1.24	40.6	0.40	14	25,727	10	72	0.335	0.677	0.500	0.74
GL3.1	1.21	42.0	3.07	28	31,662	60	67	0.412	0.785	0.447	0.57
GL3.2	1.21	42.9	2.20	28	39,088	17	64	0.446	0.696	0.536	0.77
GL3.3	1.19	44.4	1.30	28	25,718	12	65	0.449	0.645	0.624	0.97
GL3.4	1.15	50.2	0.40	28	31,682	10	67	0.438	0.763	0.585	0.77
GL4.3	1.50	22.1	1.30	7	35,226	11	57	0.347	0.259	0.541	2.09
GL4.4	1.42	30.8	0.40	7	25,728	14	54	0.409	0.313	0.583	1.86
GL5.1-2	1.60	15.5	2.30	4	25,740	14	53	0.321	0.379	0.304	0.80
GL5.2-3	1.58	17.7	1.31	4	20,883	8	55	0.321	0.209	0.498	2.39
GL5.4	1.52	23.6	0.35	4	276,824	14	85	0.118	0.487	0.293	0.60
GL12.1-2	1.44	22.1	2.55	10	23,189	15	52	0.417	0.564	0.311	0.55
GL12.3	1.47	24.1	1.55	10	43,413	11	54	0.387	0.450	0.387	0.86
GL12.4	1.39	32.7	0.45	10	25,727	17	58	0.393	0.677	0.265	0.39

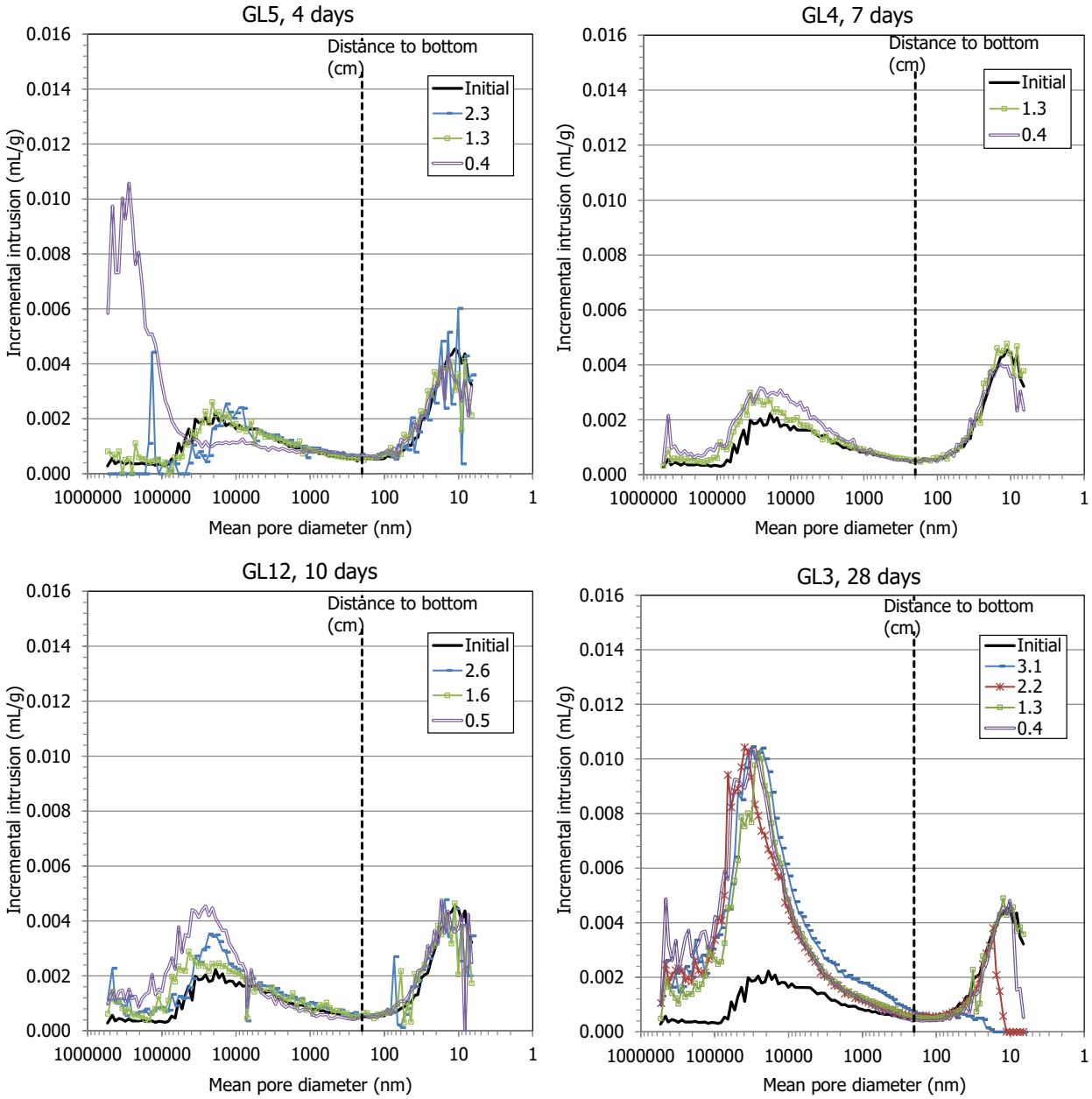

Figure A- 4. Pore size distribution of samples tested in GAP-liquid cells with saturation opposite to gap for different times and for the initial block expressed as incremental mercury intrusion

Table A- 29. Pore size distribution obtained with MIP of samples from of GAP-liquid tests saturated through gap (distance from sample bottom; e: void ratio; M: pores >200 nm; m: pores <200 nm)

Ref.	ρ_d (g/cm^3)	*w* (%)	Distance (cm)	Time (days)	Mode M (nm)	Mode m (nm)	e intruded (%)	non-intruded *e*	e_M	e_m	e_m/e_M
Initial	1.69	13.5	-	-	18,807	11	64	0.215	0.199	0.398	2.00
GL9.1	1.07	48.6	2.78	14	20,890	14	70	0.455	0.894	0.629	0.70
GL9.2	1.20	40.4	1.65	14	31,701	12	70	0.379	0.699	0.551	0.79
GL9.3	1.32	33.9	0.55	14	25,734	15	64	0.381	0.489	0.556	1.14
GL11.1	1.00	26.8	2.63	2	25,729	15	28	1.225	1.427	0.273	0.19
GL11.2int	1.56	19.0	1.60	2	43,410	17	56	0.324	0.236	0.494	2.09
GL11.2ext	1.52	19.9	1.60	2	25,741	15	51	0.382	0.214	0.562	2.62
GL11.3	1.61	16.4	0.50	2	25,724	11	56	0.301	0.210	0.467	2.23
GL13.1	1.05	52.1	3.10	39	18,803	7	67	0.518	0.785	0.447	0.57
GL13.2	1.14	46.7	2.20	39	39,130	13	65	0.474	0.696	0.536	0.77
GL13.3	1.18	42.6	1.30	39	53,617	13	56	0.566	0.645	0.624	0.97
GL13.4	1.20	42.0	0.40	39	48,299	7	62	0.474	0.763	0.585	0.77

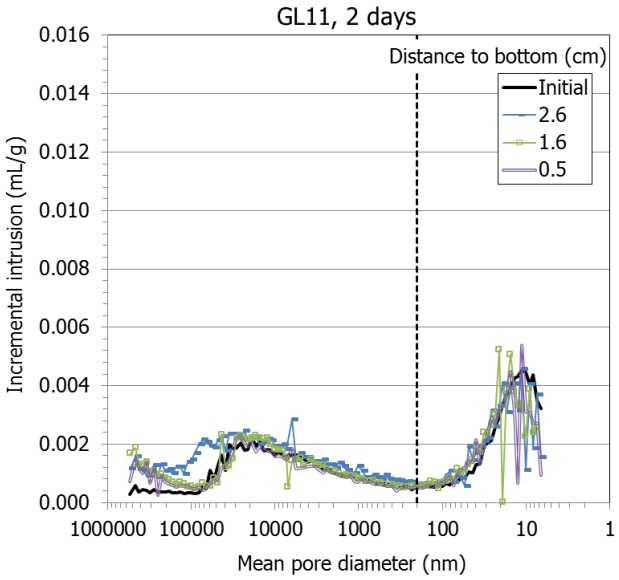

Figure A- 5. Pore size distribution of sample GL11 tested in GAP-liquid cell with saturation through the gap and for the initial block expressed as incremental mercury intrusion

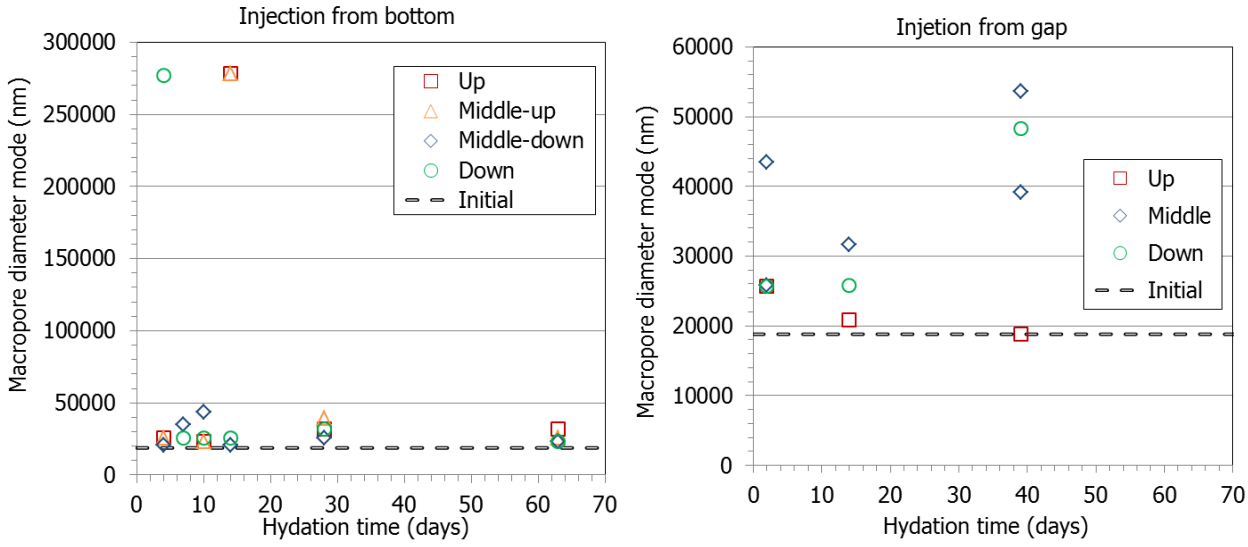

Figure A- 6. Mode size of macropores of subsamples tested in GAP-liquid cells with water injection opposite to gap (left) and from gap (right) for different times and as a function of the position of the subsample (gap on top; duplicate samples for each duration)


2695-8864